Host mRNA 3'-end processing machinery are critical binding partners during dengue virus infection

Min Jie Alvin Tan[1*], Ahmad Nazri Mohamed Naim[2], Yan Ting Lim[3], Radoslaw M. Sobota[3], Martin L. Hibberd[4] and Subhash G. Vasudevan[1]

[1] Program in Emerging Infectious Diseases, Duke-NUS Medical School, Singapore; [2] Genome Institute of Singapore, Singapore; [3] Functional Proteomics Laboratory, Institute of Molecular and Cellular Biology, Singapore; [4] Pathogen Molecular Biology, London School of Hygiene and Tropical Medicine, UK

* address correspondence to Min Jie Alvin Tan, alvin.tan@duke-nus.edu.sg

ABSTRACT

Dengue virus (DENV) causes a wide variety of dengue diseases that threaten over half of the world's population. At present, there is no antiviral therapeutics against dengue. Virus infection and its associated pathologies are the result of a myriad of interactions between the virus and its host, of which most are protein-protein interactions (PPIs). Virus-encoded proteins modulate the host environment for the virus' benefit by interacting with host proteins during infection. Thus studies of these virus-host PPIs are most informative when performed in the context of an infection. We undertook a comparative affinity purification-mass spectrometry approach to generate a DENV-host protein-protein interactome during DENV infection and identified mRNA 3'-end processing protein complexes as novel interactors of DENV NS3. We demonstrated that the presence of the cleavage and polyadenylation specificity factor complex proteins, but not their enzymatic activity, is crucial for DENV replication, thus unveiling a potential new direction for the development of host-directed antiviral therapeutics.

INTRODUCTION

Dengue virus (DENV) is estimated to infect about 400 million people worldwide every year, and over half of the world's population (3 billion people) resides in regions that are at risk from dengue (1). It is the etiological agent of a wide variety of dengue diseases ranging from mild dengue fever to severe dengue hemorrhagic fever and potentially fatal dengue shock syndrome (2). Currently, there is no approved antiviral treatment for dengue while the available vaccines are limited in efficacy and availability.

Similar to other members of the flavivirus genus, the DENV genome consist of a single-stranded positive sense RNA of ~11000 nucleotides encoding a ~3400 amino acid residue polyprotein precursor that is post-translationally cleaved into three structural proteins (capsid, pre-membrane/membrane and envelope) and seven non-structural (NS) proteins (NS1, NS2A, NS2B, NS3, NS4A, NS4B and NS5) (3). Virus replication and pathogenesis are the result of the perturbations induced in the host protein network by virus proteins during virus infection. Thus the elucidation of the virus-host interactome will be instrumental to a complete understanding of the cellular processes during a virus infection, and the consequent identification of interacting host proteins that are crucial for virus replication represent potential targets for host-directed antiviral therapeutics.

Loss-of-function genetic screens have proven useful in identifying host dependency factors that are critical for DENV replication (4-7), but whether and how these factors interact with virus proteins during virus infection and pathogenesis is

often not uncovered. In contrast, proteomic studies directly identify host proteins and pathways targeted by DENV proteins. Proteome-wide studies applying the expression of fragments of individual virus proteins using the yeast-2-hybrid (Y2H) method (8, 9) or individual full-length virus proteins using the affinity purification coupled with mass spectrometry (AP-MS) approach (10, 11) have had success in identifying host protein interactors. But they only reveal part of the story as these studies do not replicate cellular conditions during virus infection. In addition, it is known that the flavivirus proteins interact with one another during virus infection (12). Hence such studies are also missing out on DENV-host protein interactions that are mediated by multi DENV protein complexes.

Virus-host protein interactome studies in the context of virus infection have successfully identified critical interacting human proteins and pathways for influenza infection (13, 14). Similar studies in flaviviruses have been held back by a compact and highly sensitive flavivirus genome intolerant to manipulation (15), despite advances in the development of reverse genetics systems in the construction of stable flavivirus infectious DNA clone constructs (16, 17). Attempts at sequence insertions have often produced constructs that were less fit compared to wild type and/or unstable during continuous passaging in cells (17). This has limited studies using replicon and infectious DNA clone systems to interrogate the interactome of virus proteins to individual virus proteins (18, 19). Thus, it has remained a tremendous challenge to perform a virus proteome-wide study and comprehensively characterize the flavivirus-host protein interactome during virus infection.

In this study, we seek to overcome these challenges by co-expressing an epitope tagged DENV protein during virus infection. Following affinity purification and mass spectrometry, we identified about 200 host proteins as prospective interacting proteins (PIPs) of the DENV non-structural proteins. Proteins involved in the metabolism of RNA were highly enriched amongst these PIPs, with protein complexes involved in mRNA 3'-end processing pathway in particular being targeted by NS3. We further demonstrate that DENV requires the presence of the cleavage and polyadenylation specificity factor (CPSF) complex for replication in a manner separate from CPSF's endonuclease activity. Collectively, our results represent a systematic DENV-human protein interactome in the context of DENV infection that has directed the discovery of an interacting host protein complex crucial for virus replication independent of its enzymatic function. This discovery opens a new angle for the development of host-targeted antiviral therapeutics.

RESULTS

Identification of interacting host proteins during DENV infection

We first generated expression plasmids for each virus protein using the infectious clone of a clinical strain of dengue serotype 2 virus (EDEN2) as the template (20). Flavivirus proteins are translated as a polyprotein that is subsequently cleaved by both the host proteases furin and signalase on the lumen side of the ER and the viral NS2B/NS3 protease on the cytoplasmic side to yield the individual viral proteins (Fig. 1A). Hence they do not typically start with the methionine residue, except the capsid (C) protein. Considering the possible role of the N-terminal region in the insertion of NS2A and NS4A into the membrane (21, 22), we decided against adding an N-terminal methionine residue or using a N-terminal FLAG tag to initiate translation. Instead we used the ubiquitin fusion technique to express the DENV proteins with their native N-terminal residue (23, 24). The coding sequence for a HA-

tagged K48R ubiquitin (Ub) is cloned directly before the coding sequence of the flavivirus protein. Upon expression in the cell, the ubiquitin is cleaved by cellular de-ubiquitinases (DUBs), leading to the release of the DENV protein with its native N-terminal residue (Fig. 1B). Finally, we added a C-terminal FLAG tag to enable the use of a common antibody for affinity purification of all the DENV proteins. This also permits the generation of control samples that are used to normalize the background interactors during comparative analysis to identify human protein interactors specific for each DENV protein.

We then transfected these expression plasmids into Huh7 cells to verify the expression of various DENV proteins at their respective expected sizes by Western blot (Fig. 1B). Proper and complete cleavage of the HA-Ub molecule from the DENV proteins was also confirmed (Supplementary Fig. 1). The characteristic polyubiquitin smear was observed in all the samples, except the empty vector and capsid samples, as the capsid (C) expression plasmid (second lane) was not cloned with a HA-Ub sequence since it has a native methionine.

Having established the correct expression of each virus protein, we proceeded to prepare samples for the mass spectrometry experiments. We transfected the respective plasmids individually into Huh7 cells, followed 6 hours later by infection of the cells with DENV (Fig. 1C). The FLAG-tagged bait proteins were then extracted for affinity purification 48 hours post-infection before being sent for identification by mass spectrometry together with their associated proteins. We generated triplicate affinity purification samples for each DENV bait protein but were unable to reliably detect the bait proteins in some of these replicate samples (e.g. one of the triplicates for NS2B). After omitting these replicates from our analysis, thousands of host proteins were collectively identified as being associated with the DENV bait proteins (Supplementary Table 1).

To facilitate the identification of reproducible and DENV bait protein specific interacting host proteins, we analyzed the replicate samples for each DENV bait protein using two different scoring algorithms on the Resource for Evaluation of Protein Interaction Networks (REPRINT) platform: Contaminant Repository for Affinity Purification (CRAPome) and Significance Analysis of INTeractome (SAINT) (25, 26) (Supplementary Table 1). Both algorithms compare the spectral counts of proteins detected in the respective replicate bait DENV protein samples to negative control samples generated under the same affinity purification conditions to produce an enrichment (FC for CRAPome) or probability (SP for SAINT) score.

This dataset represents a comprehensive database of the DENV-human protein interactome in the context of DENV infection. Hence we were first interested to see the number and frequency of DENV proteins for each of the bait DENV proteins (Fig. 1D). We detected extensive interactions between the DENV proteins, including previously described interactions such as those between NS3 and NS5 (27, 28), NS4A and NS4B (29), NS1 and NS4A (30, 31), and NS2A and C (32). While this is unsurprising considering that all the non-structural proteins come together to form the replication complex (33), further studies are necessary to investigate the significance and context of these interactions. In particular, we detected a strong reciprocal interaction between the E and NS2B proteins that is likely to be occurring outside the context of the replication complex. We also noted that none of the detected DENV proteins scored as significant on either CRAPome (FC ≥ 4) or SAINT (SP ≥ 0.9) (Supplementary Table 2), suggesting that such interactions make up a relatively small proportion of the interactions that DENV proteins make during virus infection.

152 To increase the stringency in identifying human interacting proteins unique to
153 each bait DENV protein, we examined the scores assigned by SAINT to the human
154 proteins and identified about 200 proteins that were scored as significant (SP ≥ 0.9)
155 in at least two of the three replicate samples of a bait DENV protein. We termed
156 these proteins as prospective interacting proteins (PIPs) and found that they were
157 well distributed amongst the various non-structural proteins (Fig 1E). In addition,
158 more than half of the proteins that were found in all three replicates have been
159 previously identified as an interactor or differentially expressed during DENV
160 infection (Supplementary Table 3), validating the effectiveness of our approach in
161 identifying true interacting proteins.
162
163 **DENV proteins interact with host proteins involved in diverse host pathways**
164 When we visualized the list of PIPs in a DENV-human protein interaction map,
165 we found that there were numerous human proteins that were identified as PIPs of
166 more than one DENV protein (Fig. 2A). This finding stands out from previous
167 proteomic studies in which there were few overlapping interacting proteins identified
168 between the virus proteins (10, 11, 34), and could be attributed to our study being
169 performed in the context of DENV infection that enabled the identification of host
170 proteins binding to DENV protein complexes such as the virus replication complex.
171 We next performed pathway enrichment analysis to identify host pathways
172 that are enriched in the list of PIPs. We found these proteins to be involved in
173 diverse host processes (Supplementary Table 4), with the most significant
174 enrichment in the proteins associated with the chaperonin containing tailless
175 complex polyprotein 1 (CCT) complex (green), along with proteins involved in
176 diverse host processes including RNA metabolism (yellow) and asparagine-linked
177 glycosylation (red) (Fig. 2A and 2B, and Supplementary Table 4).
178 Two previous studies have performed AP-MS studies by incorporating epitope
179 tags into the NS1 and NS5 gene in the context of a replicon or infectious clone (18,
180 19). To compare our respective approaches, we performed pathway enrichment
181 analysis on the human proteins that were identified in both NS1 and NS5 datasets.
182 We found both lists of identified proteins to be significantly enriched in the same
183 pathways (Fig. 2C and Supplementary Tables 5 and 6). In particular, the CCT
184 complex (Formation of tubulin folding intermediates by CCT/TriC) was significantly
185 enriched in both NS1 lists (Fig. 2C, left) while mRNA metabolic process, mRNA
186 processing and ribonucleoprotein complex biogenesis were most significantly
187 featured in both NS5 lists (Fig. 2C, right). Taken together, our approach compares
188 favorably in the identification of human protein interactors with the reverse genetics
189 approach that directly incorporates an epitope tag into the virus genome.
190 Finally, we checked that our exogenously expressed FLAG-tagged DENV
191 proteins are localizing to their appropriate cellular compartments. We used the gene
192 ontology (GO) cellular components database to analyze the list of interacting
193 proteins for three DENV proteins (NS4A, NS4B and NS5) with previously defined
194 subcellular localization (Supplementary Table 7). The top three terms for NS5 were
195 ribonucleoprotein complex, nuclear specks and catalytic step 2 spliceosome (Fig.
196 2D), which is expected with DENV2 NS5 being an RNA-dependent RNA
197 polymerase, its known localization to the nucleus (35) and its ability to interact with
198 and modulate splicesome activity (19). Consistent with DENV NS4B protein's
199 reported localization to the mitochondria and modulation of mitochondrial structure
200 (36, 37), the top hit from the GO cellular components analysis was the mitochondrial
201 matrix (Fig. 2E). Finally the vesicle lumen was amongst the top hits for both

membrane-bound NS4A and NS4B (Fig. 2E). The results of these analyses suggest that the expressed DENV proteins are localizing to their native cellular components within the cell and interacting with previously reported host proteins.

Collectively, we have generated a comprehensive DENV-human protein interactome in the context of DENV infection and identified host proteins and pathways targeted by DENV non-structural proteins during infection.

Oligosaccharyltransferase (OST) complex members are a common interactor of DENV non-structural (NS) proteins

Asparagine-linked glycosylation was one of the top terms picked up by pathway enrichment analysis and is catalyzed by the oligosaccharyltransferase (OST) complex (Fig. 2B). The OST complex is an essential human host protein complex for flavivirus infection (4, 5, 38), although the nature of its interaction with the flavivirus proteins during virus infection has not been fully characterized. We detected peptides from many members of the OST complex with varying frequency and abundance in the AP-MS samples from the various DENV proteins (Supplementary Table 8). CRAPome and SAINT analysis revealed that the OST complex members were more frequently and significantly enriched in samples from the DENV non-structural proteins than the structural proteins (Fig. 3A and Supplementary Table 8). In addition, the membrane-bound NS proteins (NS1, NS2A, NS2B, NS4A and NS4B) pulled down the OST complex members with greater frequency and abundance, with NS4A interacting with the greatest number of complex members.

We sought to validate some of these interactions by immunoprecipitation followed by Western blot (Fig. 3B). We co-transfected V5-tagged members of the OST complex and FLAG-tagged DENV2 NS4A and NS4B, and performed reverse immunoprecipitation using V5 antibodies, followed by Western blotting. Consistent with our AP-MS data, DENV2 NS4A was pulled down by DDOST, RPN1, RPN2 and STT3A (Fig. 3B, left). Interestingly, DENV NS4B was also pulled down by the same set of proteins (Fig. 3B, right).

DENV replication takes place in virus replication organelles containing double-stranded RNA and the virus replication complex (RC) made up of all the DENV NS proteins (33, 39, 40). The high frequency of OST complex members as interactors of DENV NS proteins suggests that the interaction between DENV and the OST complex could be taking place in the context of these virus replication organelles. We examined the intracellular localization of the OST complex members RPN1 and MAGT1, and the virus RC by immunofluorescence assay (Fig. 3C). We found a strong co-localization of dsRNA with both RPN1 and MAGT1 in Huh7 cells infected with DENV, thus putting the OST complex in close proximity of the virus replication organelle. Taken together, our data supports a model in which the OST complex is recruited via interactions with DENV proteins within the DENV RC to the DENV virus replication organelle during virus infection.

DENV NS3 interacts with and re-localizes CPSF complex proteins

RNA metabolism was the second most-enriched pathway amongst the host proteins in our DENV-human protein interactome (Fig. 2B). Amongst the DENV proteins, DENV NS3 is a multi-functional protein with helicase and nucleoside 5'-triphosphate activities. Hence, we analyzed the list of human proteins identified in our NS3 samples and found that metabolism of RNA, in particular mRNA, was the most enriched term (Fig. 4A and Supplementary Table 9). Within the list of proteins

252 associated with this term were members of protein complexes involved in mRNA 3'-
253 end processing. Besides the core U5 snRNP components of the spliceosome that
254 had previously been identified as a target of NS5 (19), we also detected member
255 proteins of the cleavage stimulation factor (CSTF), cleavage factor (CF), and the
256 cleavage and polyadenylation specificity factor (CPSF) complexes (Fig. 4B).
257 Intriguingly, some of these proteins were also detected with lower CRAPome
258 enrichment scores in our DENV NS5 samples, suggesting that both NS3 and NS5
259 could be involved in interacting with members of this pathway (Fig. 4C and
260 Supplementary Table 10).
261 We next sought to confirm these interactions by co-expressing DENV NS
262 proteins with CPSF3, CPSF4 or the spliceosome protein EFTUD2 in 293T cells.
263 After immunoprecipitation and Western blotting, we found that NS3 and NS5, but not
264 NS1, can be pulled down by CPSF3, CPSF4 or EFTUD2 (Fig. 4D). This is in line
265 with our mass spectrometry results, demonstrating a specific interaction between
266 NS3 and NS5, and proteins involved in RNA metabolism.
267 Since all six members of the CPSF complex were detected in our NS3
268 samples, we chose to investigate the functional implication of this interaction. We
269 first examined the subcellular localization of CPSF3 and CPSF4 during DENV
270 infection using an immunofluorescence assay (IFA) (Fig. 5A). CPSF3 and CPSF4
271 were primarily localized in the nucleus, but we observed a decrease in the levels of
272 CPSF proteins in DENV-infected Huh7 cells that were co-stained with DENV NS3
273 (Fig. 5A and 5B) or dsRNA (Extended Data 1A). Quantification of the fluorescent
274 intensity revealed a significant decrease in the CPSF protein levels in the nucleus,
275 and a small but significant increase in CPSF protein levels in the cytoplasm (Fig.
276 5B). To investigate whether DENV NS3 alone is sufficient to re-localize the CPSF
277 proteins, we expressed DENV NS3 in Huh7 cells and performed the same IFA. We
278 found that Huh7 cells expressing NS3 also exhibited a significant re-localization of
279 the CPSF proteins from the nucleus to the cytoplasm (Fig 5C and 5D). In contrast,
280 DENV NS1 did not have a significant effect in the subcellular localization of the
281 CPSF proteins (Extended Data Fig 1B).
282
283 **The CPSF complex, but not its endonuclease activity, is important of flavivirus**
284 **replication**
285 CPSF3 is the endonuclease responsible for the CPSF complex's function of
286 cleaving pre-mRNA before polyadenylation during the maturation of host mRNA (41).
287 It has also been shown to be a promising drug target in some cancers and parasites
288 (42). Influenza virus and herpes simplex virus disrupt CPSF complex functions via
289 interactions with their respective encoded virus proteins (43). Hence we examined
290 whether DENV NS3 and NS5 have an effect on the pre-mRNA 3'-end processing
291 (44). We found that expression of DENV NS3 and/or NS5 did not have an effect of
292 IL8 pre-mRNA processing. In comparison, treatment of cells with the CPSF3
293 enzymatic inhibitor JTE-607 led to a significant accumulation of IL8 pre-mRNA
294 (Extended Data Fig. 2).
295 We next investigated whether the CPSF complex plays a role in DENV
296 replication. We used RNA interference (RNAi) to knock down CPSF3 expression
297 levels and then infected the cells to interrogate the importance of the CPSF complex
298 in DENV replication. Using two unique small interfering RNAs (siRNAs) against
299 CPSF3, we found a significant reduction in virus RNA replication (Fig. 6A). In
300 addition, this reduction is dose-dependent, as increasing amounts of transfected

301 siRNA that corresponded with reductions in the levels of CPSF3 RNA and protein led
302 to decreasing amounts of virus RNA replication and virus production (Fig. 6B).
303 The OST and CCT complexes have been previously found to be crucial pan-
304 flavivirus host factors. Hence we examined whether the CPSF complex is also
305 important for ZIKV infection. When we knocked down expression of CPSF3 with the
306 same CPSF3 siRNAs, we found that ZIKV replication is also abrogated (Fig. 6C). We
307 then investigated whether the CPSF complex is targeted in a similar manner by ZIKV
308 by testing whether ZIKV NS3 also interacts with CPSF3. We co-transfected V5-
309 tagged CPSF3 with FLAG-tagged DENV and ZIKV NS3, and subjected the cell
310 lysates to immunoprecipitation and Western blotting. We found that ZIKV NS3, like
311 DENV NS3, is also able to interact with CPSF3, suggesting a common mode of
312 targeting the CPSF complex amongst the flaviviruses (Fig. 6D).
313 JTE-607 is a small molecule inhibitor of the CPSF complex that binds to
314 CPSF3 and blocks its endonuclease activity at 10μM (44, 45). We found that JTE-
315 607 has very low toxicity with little effect on cell viability up to 250μM (Fig. 6E). We
316 next tested the effect of JTE-607 on DENV replication and found that JTE-607 had
317 no effect on DENV replication at an inhibitory concentration of 10μM (Fig. 6F, left).
318 But we found that JTE-607 becomes effective in inhibiting DENV replication as we
319 increased the concentration up to 250μM in our dose-response study, with an
320 estimated 50% effective concentration (EC50) of ~175μM (Fig. 6F). When we sought
321 to understand the cause of this inhibition, we found a dose-dependent decrease in
322 CPSF3 levels with increasing concentration of JTE-607 treatment. Interestingly,
323 CPSF4 levels also decreased in a similar manner (Fig. 6F), suggesting that a
324 decrease in CPSF complex levels is responsible for the observed inhibition.
325 Taken together, DENV targets the CPSF complex during DENV infection and
326 re-localized CPSF proteins to the cytoplasm. The enzymatic function of the CPSF
327 complex is not targeted by DENV and does not play a role in this abrogation, as
328 inhibition of CPSF3's endonuclease activity with a small molecule inhibitor has no
329 effect on DENV replication. But a reduction in CPSF complex protein levels, whether
330 by RNA interference or chemical treatment, leads to an abrogation of DENV
331 replication
332
333 **DISCUSSION**
334 During virus infection, virus proteins disrupt host protein networks to promote
335 virus replication and pathogenesis. Hence the revelation of the virus-host
336 interactome is a critical piece in uncovering the cellular processes that occur during a
337 virus infection. Previous proteomic studies on DENV have been limited to studying a
338 single DENV protein in the context of DENV infection or the study of the DENV
339 proteins in the absence of DENV infection. Here we co-expressed epitope-tagged
340 DENV proteins during DENV infection to generate a comprehensive DENV-human
341 protein interactome in the context of DENV infection using an affinity purification-
342 mass spectrometry approach (Fig. 1C). We identified about 200 human proteins as
343 prospective interacting proteins (PIPs) of the non-structural (NS) proteins of DENV.
344 Pathway enrichment analysis of these proteins reveals an enrichment of members of
345 the chaperonin containing tailless complex polyprotein 1 (CCT) complex, and
346 proteins involved in asparagine N-linked glycosylation and RNA metabolism (Fig.
347 2B).
348 The primary protein complexes responsible for the former two pathways have
349 have been previously reported to be crucial host factors for DENV replication. The

oligosaccharyltransferase (OST) complex catalyzes the co-translational glycosylation of specific asparagine residues, and had been previously identified to be an indispensable human host protein complex for flavivirus infection via genetic and genomic studies (4, 5, 38). But the nature of its interaction with the virus at a protein level had been incomplete and seemingly conflicting. We clarify this by detecting members of the OST complex in our AP-MS samples for every single non-structural (NS) DENV protein (Fig. 3A) and showing co-localization of OST complex members with dsRNA in DENV-infected cells (Fig. 3C). Taken together, these data suggest that the interaction with the OST complex is taking place in the context of the virus replication complex within the virus replication organelles. In contrast, the CCT/TRiC complex is only targeted by the NS1 protein as members of the CCT complex were only scored as PIPs for NS1. This was confirmed via immunoprecipitation followed by Western blotting, as NS1, but not NS3 or NS5, is able to pull down CCT2 and CCT7 (Extended Data Fig. 3 and Supplementary Table 11).

The RNA metabolism pathway comprises all the steps in which RNA transcription products are further modified to yield mature mRNA, including capping, splicing, 3'-cleavage and polyadenylation. We found members of protein complexes involved in splicing and mRNA 3'-end cleavage in the AP-MS samples for NS3 and NS5. In particular, we identified and validated members of the CPSF complex as novel interactors of NS3 (Fig. 4). DENV infection and the expression of DENV NS3 alone is sufficient to re-localize CPSF proteins from the nucleus, suggesting a recruitment of CPSF proteins to the cytoplasm where virus replication occurs (Fig. 5). When CPSF3 expression is knocked down using RNA interference, DENV replication was abrogated in a dose-dependent manner, indicating the importance of the CPSF complex during virus replication (Fig. 6B). The endonuclease function of CPSF3 is not involved in this role, as a small molecule inhibitor JTE-607 has no effect on DENV replication at enzyme-inhibitory concentrations (Fig. 6E). Intriguingly, we found that higher concentrations of JTE-607 led to an abrogation of DENV replication that corresponded to a reduction in the protein levels of not only CPSF3 but also CPSF4. Taken together, our results demonstrate that the presence of the CPSF complex proteins is critical for DENV replication and support a model in which DENV is targeting and recruiting the CPSF complex, but not its enzymatic activity, during virus replication.

The identification of host targets for antiviral therapeutics have been driven by genetic and small molecule inhibitor screens that have largely limited discovery to non-essential and enzymatic proteins respectively. Using a proteomic approach, we have identified a host protein complex that is crucial for DENV infection independent of its enzymatic activity. This raises the possibility of targeting essential enzymatic proteins for antiviral therapeutics by disrupting the interaction between the virus and human protein without affecting the host protein's enzymatic activity. The potential of such an approach had been recently demonstrated in an inadvertent manner in the discovery of a dengue virus inhibitor that was subsequently found to target the NS3-NS4B interaction (46). We have found that the helicase domain of NS3 is sufficient to mediate the interaction with an N-terminal fragment of CPSF3 (Extended Data Figure 4). This finding lays the foundation for further structure-function studies necessary to uncover the molecular mechanism of the interaction, and to direct the development of specific small molecules to disrupt this interaction.

ACKNOWLEDGEMENTS

We thank members of the Vasudevan and Sobota laboratories for discussion, advice and reagents. This work was supported by National Medical Research Council grants NMRC/OFYIRG/0006/2016 to M.J.A.T. and NMRC/CBRG/0103/2016 to S.G.V., and Ministry of Health grants MOH-000086 (MOH-OFIRG18may-0006/2019) and MOH-001497 (MOH-OFIRG23jul-0004) to S.G.V.

AUTHOR CONTRIBUTIONS

M.J.A.T. and A.N.M.N. performed the cloning and affinity purification of the dengue virus proteins. Y.T.L and R.M.S. performed mass spectrometry and initial data analysis. M.J.A.T. performed the subsequent Metascape analysis and downstream biological assays. M.J.A.T., S.G.V. and M.L.H. supervised the research. M.J.A.T. wrote the manuscript with input from S.G.V and M.L.H.

DISCLOSURE AND COMPETING INTERESTS STATEMENT

The authors declare that they have no conflict of interest.

METHODS

Cell lines and viruses. Huh-7 and 293T (ATCC) were maintained in high-glucose Dulbecco's modified Eagle's medium (DMEM) containing L-glutamine supplemented with 10% [v/v] fetal bovine serum (FBS) and 1% [v/v] penicillin and streptomycin (P/S). BHK-21 cells (ATCC) were maintained in RPMI1640 medium supplemented with 10% FBS and 1% P/S. All cells were grown at 37°C in 5% CO_2. C6/36 cells (ATCC) were maintained in RPMI1640 medium supplemented with 25 mM HEPES, 10% FBS and 1% P/S at 28°C, in the absence of CO_2.

The two ZIKV strains, H/PF/2013 (KJ776791.2) and Paraiba01/2015 (KX280026.1), used in this study were grown in C6/36 cells, titered in BHK-21 cells and stored at -80°C (47)

The DENV strain (GenBank accessions: DENV2, EU081177) was obtained from the Early Dengue infection and outcome (EDEN) study (48). The ZIKV strain H/PF/2013 (GenBank accession: KJ776791.2) was a gift from Cécile Baronti at Aix Marseille Université (47). The viruses used in this study were grown in C6/36 cells, titered in BHK-21 cells and stored at -80°C. Institutional approval has been granted by Duke-NUS Medical School to perform experiments with DENV and ZIKV.

Plasmid construction

The virus protein expression plasmids were generated from the DENV2 infectious clone plasmid (35) for the DENV strain. The list of primers used for plasmid cloning are listed in Supplementary Table 12. The expression plasmids for the human genes were obtained from the CCSB-Broad Lentiviral Expression Library (PerkinElmer) (49).

439 **Plasmid transfection and virus infection**

440 For immunoprecipitation assays, 1.5e5 Huh7 cells were seeded onto 12-well plates and incubated
441 overnight at 37°C with 5% CO_2. Cells were transfected with 1µg of the indicated plasmids using
442 FuGENE 6 (Promega), according to the manufacturer's protocol.

443 For immunofluorescence assays, 1.5e5 Huh7 cells were seeded onto 12-well plates containing #1.0
444 glass cover slips, and incubated overnight at 37°C with 5% CO_2. Cells were transfected with 1µg of the
445 indicated plasmid using FuGENE 6 (Promega), according to the manufacturer's protocol. For virus
446 infection, cells were incubated with 500µl of virus inoculum at the indicated MOI for 1h, and viral
447 inoculums were replaced with growth media prior to 24h incubation at 37°C with 5% CO_2.

448 **Immunofluorescence assay and confocal laser scanning microscopy**

449 The cells on coverslips were fixed with 4% paraformaldehyde for 15min at room temperature, washed
450 with 1x phosphate-buffered saline (PBS) buffer followed by blocking and permeabilization using 2%
451 [w/v] bovine serum albumin (BSA)/0.3% [v/v] Triton X-100/PBS for 1h at room temperature. Cells were
452 washed with 1x PBS before incubation with the following primary antibodies: dsRNA (1001050;
453 Exalpha), DENV NS3 (3F8) (50), CPSF3 (H00051692-M01; Novus Biologicals), CPSF4 (15023-1-AP;
454 Proteintech), RPN1 (198598; Abcam) and MAGT1 (17430-1-AP; Proteintech). After washing with 1x
455 PBS, the cells were incubated with the following secondary antibody coupled to Alexa-Fluor 488 and
456 594 (Thermo Fisher). Cell nuclei were visualized using DAPI (D9542; Merck). Coverslips were mounted
457 using ProLong Gold Antifade reagent (Thermo Fisher) onto glass slides and confocal laser scanning
458 microscopy was performed using a Zeiss LSM 710 upright confocal microscope (Carl Zeiss, Germany)
459 with a 63x 1.35 NA objective. Image processing was performed with Zeiss ZEN and ImageJ software
460 (51).

461 **Affinity purification-mass spectrometry sample preparation.** 2.5e6 Huh7 cells were transfected
462 with 10µg of empty vector or FLAG-tagged DENV proteins. 6h post-transfection, the cells were
463 infected with DENV as above. 48h post-infection, cells were washed twice with PBS, and lysed with
464 0.5% NP-40 lysis buffer (50mM Tris-HCl pH 7.8, 150mM NaCl) or 0.5% DDM lysis buffer (20mM Tris-
465 HCl pH 7.5, 100mM NaCl). Affinity purification was performed using anti-FLAG antibody (F1804;
466 Merck) and SureBeads Protein A/G Magnetic Beads (Bio-Rad)

467 **Mass spectrometry.** Bound proteins were reduced with 20mM TCEP for 20min at 55°C and alkylated
468 with 55 mM 2-chloroacetamide (CAA) for 30 min, in the dark, at room temperature. Before digestion,

469 samples were diluted with 100 mM triethylamonium bicarbonate buffer (TEAB). Protease digestion was
470 carried out with LysC enzyme (Wako) for 4 h, followed by trypsin (Promega) treatment for 18 h at 25°C
471 (1:100, enzyme:protein ratio). Subsequently, samples were acidified with 1% trifluoroacetic acid and
472 peptides were desalted with Sep-Pak C18 cartridges (Waters). Elution of peptides was performed with
473 0.5% acetic acid, 80% acetonitrile followed by peptide concentration using a vacuum concentrator
474 system (Eppendorf).
475 **Mass spectrometry acquisition and data processing.** Digested peptide samples were loaded on a
476 heated (50°C) Easy-Spray 75µm x 50cm column (Thermo Scientific) on an EASY-nLC 1000 system
477 coupled to a Fusion Mass Spectrometer (Thermo Scientific) with an EASY-Spray source. Peptides were
478 separated over a 100 min gradient, using mobile phase A (0.1% formic acid in water) and mobile phase
479 B (0.1% formic acid in 95% acetonitrile). Mass spectra were collected in data-dependent mode with
480 cycle time of 3s between master scans. MS1 scans were performed in the Orbitrap with 120K resolution,
481 AGC target of 400,000 and maximum injection time of 100ms. MS/MS collision induced dissociation
482 was performed in the ion trap, with collision energy at 35 %, isolation window of 1.0 m/z, AGC target of
483 8,000, and maximum injection time of 70ms.
484 Mass spectra raw files were searched with Mascot in Proteome Discoverer 2.4 against a human uniprot
485 database (retrieved in 2016), with following parameters: precursor mass tolerance of 10ppm, fragment
486 mass tolerance of 0.8 Da, trypsin as enzyme with maximum 3 missed cleavages, with static modification
487 for carbamidomethyl (C), and dynamic modifications for acetyl (Protein N-terminus), oxidation (M) and
488 deamidation (N,Q). False discovery rate estimation with 2 levels: Strict = FDR 1%, Medium = FDR 5%.
489 Precursor mass peak (MS1) intensities were quantified by label-free quantification (LFQ) using the
490 Minora feature detector.
491 **Data availability.** The raw spectra and search data will be uploaded to the Japan ProteOme STandard
492 Repository (jPOSTrepo).
493 **Interactome analysis.** The lists of detected proteins for each DENV bait protein was analyzed on the
494 Resource for Evaluation of Protein Interaction Networks (REPRINT) platform using the Significance
495 Analysis of Interactome (SAINT) and Contaminant Repository for Affinity Purification (CRAPome)
496 analysis tools (25, 26), and prey proteins with a SAINT score ≥ 0.9 in more than two of the three
497 replicates for its DENV bait protein were designated as prospective interacting proteins (PIPs). The

498 DENV-host protein interactome was visualized using Cytoscape (52). The complete details of the
499 analyses are provided in the supplementary data (Supplementary Table S6).
500 **Enrichment analysis.** Each list of candidate interacting proteins was analyzed with a number of
501 ontology sources including KEGG pathway, gene ontology biological processes, CORUM, reactome
502 gene sets and gene ontology cellular components. All the pathway enrichment analysis and
503 visualizations were performed using Metascape (http://metascape.org/gp/index.html#/main/step1) (53).
504 The complete lists containing the terms, results and statistics for all the Metascape analyses are
505 provided in Supplementary Information.
506 **RNA extraction and RT-qPCR.** Total RNA from cell lysates was isolated using the RNeasy kit (Qiagen)
507 and subjected to cDNA synthesis using the High-Capacity cDNA Reverse Transcription Kit (Thermo
508 Fisher) according to manufacturer's instructions. RT-qPCR was conducted using the iQ SYBR Green
509 Supermix (Bio-Rad) for detection of the indicated genes. Gene expression was normalized to RPLP1
510 expression and presented as a percentage relative to empty vector control (for the pre-mRNA assay)
511 or untreated control (for DENV and ZIKV infection). The primers used for RT-qPCR are listed in
512 Supplementary Table 12.
513 **Western blotting.** Proteins were separated using NuPAGE Bis-Tris gels (Thermo Fisher Scientific) and
514 transferred onto PVDF membranes (Merck). After blocking in 4% [w/v] BSA/0.05% [v/v] Tween-20/PBS,
515 blots were incubated with the following primary antibodies diluted in 2% [w/v] BSA/0.05% [v/v] Tween-
516 20/PBS: actin (MAB1501; Merck), V5 (13202; Cell Signaling), FLAG (F1804; Merck), HA (ROAHAHA;
517 Merck), CPSF3 (H00051692-M01; Novus Biologicals), CPSF4 (15023-1-AP; Proteintech) and NS5
518 (GTX133327; GeneTex). Bound primary antibodies were incubated with AffiniPure donkey anti-rat,
519 mouse or rabbit Alexa Fluor 680 or 790 secondary antibodies (Jackson ImmunoResearch), followed by
520 visualization using the Odyssey CLx Imaging System (Li-Cor).
521 **Cell viability and virus inhibition assays.** $2x10^4$ Huh7 cells were seeded onto a 96-well white opaque
522 plate (Grenier) and treated with JTE-607 at the indicated concentrations for 24h. Cytotoxicity was
523 determined using the CellTiter-Glo Luminescent Cell Viability Assay (Promega) according to
524 manufacturer's instructions. The cell viability curve is presented as a percentage of the luminescence
525 units detected from the treated sample to that of the untreated control sample. $1x10^5$ Huh7 cells were
526 infected with DENV at MOI 1 (multiplicity of infection) for 1h, followed by treatment with the compounds
527 at the indicated concentrations for 24h. Supernatants were collected, clarified and subjected to plaque

528 quantification. The efficacy of JTE-607 (EC50: concentration at which the virus infection is reduced by
529 50%) was determined by the sigmoidal dose response curve of virus titer against drug concentration
530 using Prism (GraphPad).

531 **siRNA experiments.** $1x10^5$ Huh7 cells were transfected with the indicated concentration of siRNA
532 using DharmaFECT 1 (Horizon) for 24h before infection with DENV at MOI 1 for an additional 24h.
533 Supernatants were collected, clarified and subjected to plaque quantification 48h post transfection,
534 while RNA was extracted from the cells for RT-qPCR analysis. The ON-TARGETplus CPSF3 siRNA
535 (J-006365-09-0002 and J-006365-10-0002) were purchased from Horizon.

536 **Plaque assay.** $2x10^5$ BHK-21 cells were seeded onto a 24-well plate and incubated overnight at 37°C
537 with 5% CO_2. Virus samples were diluted with RPMI 1640 serum-free media and the cells were
538 incubated with the diluted inoculum for 1h. Virus inoculum was then removed, and the cells were
539 overlaid with 0.8% carboxylmethyl cellulose (CMC) and further incubated for 4 (for ZIKV) or 5 (for
540 DENV) days. The cells were then fixed with 3.7% formaldehyde and stained with 1% crystal violet for
541 plaque visualization.

542 **Statistical analysis.** The error bars in the figures represent the standard error of mean for each set of
543 data calculated using Prism (GraphPad). The statistical significance of the differences between the
544 various experimental conditions and the control was evaluated by the indicated statistical tests using
545 Prism (GraphPad). Data from at least two biological replicate experiments were used in the statistical
546 tests, and P values ≤ 0.05 were considered to be statistically significant.

547 **FIGURE LEGENDS**

548 **Fig. 1. Building a virus-human protein interactome during dengue virus (DENV)**
549 **infection. a.** The DENV genome is translated as a single polyprotein that is post-
550 translationally cleaved by host and DENV proteases to produce 10 DENV proteins.
551 **b**. Cloning strategy for the expression of DENV proteins with their native N-terminal
552 residue. The coding sequence for a HA-tagged K48R ubiquitin is cloned directly
553 before the coding sequence of the flavivirus protein. Upon expression in the cell, the
554 ubiquitin is cleaved by cellular de-ubiquitinases (DUBs), leading to the release of the
555 flavivirus protein with the native N-terminal residue. Western blot showing the
556 expression of the FLAG-tagged DENV proteins at their expected sizes after transient
557 transfection in Huh7 cells (below). **c**. Schematic of the experimental setup for the co-
558 expression of a FLAG-tagged DENV protein during DENV infection, followed by
559 affinity purification-mass spectrometry and REPRINT analysis to score identified
560 proteins. **d**. Heatmap depicting the average CRAPome scores of detected DENV
561 proteins from the biological replicates of each bait DENV protein, relative to the
562 average CRAPome score for that bait DENV protein. **e**. Bar graph showing the
563 number of prospective interacting proteins (PIPs) identified for each DENV non-
564 structural protein based on their SAINT scores.

565
566 **Fig. 2. The DENV-human protein interaction map during DENV infection. a**. The
567 prospective interacting proteins (PIPs) (grey) of all the DENV non-structural proteins
568 were used to construct this DENV-human protein interaction map during DENV
569 infection. The blue nodes represent the bait DENV proteins while the green, yellow
570 and red nodes highlight the human proteins associated with the CCT complex, RNA
571 metabolism and asparagine N-linked glycosylation respectively. In addition, the
572 proteins that make up the core CCT and OST protein complexes are boxed. Dotted
573 and solid lines represent interactions scored as significant by SAINT in two or three
574 biological replicates respectively. **b**. Bar graph showing the top three enriched
575 pathways associated with the PIPs for all the DENV NS proteins. **c**. Heat map
576 depicting the enriched pathways associated with human proteins pulled down by
577 DENV NS1 (left) and NS5 (right) in this and previous studies. **d**. Bar graph showing
578 the enriched cellular compartments associated with NS5 candidate interacting
579 proteins using the Gene Ontology Cellular Components database. **e**. Heat map
580 showing the enriched cellular compartments associated with NS4A and NS4B
581 candidate interacting proteins using the Gene Ontology Cellular Components
582 database. All the pathway enrichment data was generated with the Metascape
583 analysis tool searching the Gene Ontology Biological Processes, CORUM,
584 Reactome Gene Sets, KEGG Pathway and WikiPathways databases for b and c,
585 and the Gene Ontology Cellular Components database for d and e. The magnitude
586 of the bars (b and d) and the color intensity (c and e) represents the statistical
587 significance of association to the respective pathways ($-\log_{10}(P)$).
588
589 **Fig. 3. OST complex interacts with the DENV replication complex in virus**
590 **replication organelles. a**. Heat map depicting the average CRAPome scores of the
591 detected OST complex members from the biological replicates of each bait DENV
592 protein. **b**. V5 immunoprecipitation of 293T cells transfected with the indicated
593 FLAG-tagged DENV proteins and V5-tagged OST complex members, followed by
594 Western blotting with the indicated antibodies. **c**. Immunofluorescence assay of
595 Huh7 cells infected with DENV showing the localization of dsRNA (red) and the
596 indicated OST complex protein (green). The cells were imaged using Zeiss LSM 710
597 upright confocal microscope with a 63x 1.35 NA objective. The quantification and co-
598 localization of the fluorescent intensities for the DENV and OST complex protein
599 were performed using the Zeiss ZEN software Profile function, with the line-scan
600 profile being graphed using Prism. The images are representative of similar results
601 from three independent biological experiments.
602
603 **Fig. 4. DENV targets proteins involved in multiple steps during RNA**
604 **metabolism. a**. Bar graph showing the enriched pathways associated with the
605 human proteins identified in the DENV NS3 samples. Metascape analysis was
606 performed as in Figure 2. **b**. Protein-protein interaction network showing the
607 interaction between NS3 and human protein complexes involved in mRNA cleavage,
608 polyadenylation and splicing processes. The presence of an edge denotes the
609 detection of the human protein in the NS3 samples, and the thickness of the edge
610 represents the average CRAPome score of the interaction from the replicate
611 samples for NS3. **c**. Heat map depicting the average CRAPome scores of the CPSF
612 and U5 spliceosome complex members detected in the DENV NS3 and NS5
613 samples. **d**. V5 immunoprecipitation of 293T cells transfected with the indicated
614 FLAG-tagged DENV proteins and V5-tagged proteins involved in RNA metabolism,

615 followed by Western blotting with the indicated antibodies showing the specific
616 interaction between CPSF3, CPSF4 and EFTUD2, and DENV NS3 and NS5.
617
618 **Fig. 5. DENV NS3 relocalizes CPSF proteins from the nucleus to the cytoplasm**.
619 **a.** Immunofluorescence assay of Huh7 cells infected with DENV showing intracellular
620 distribution of CPSF3 or CPSF4 (green) with infected cells indicated by staining with
621 NS3 (red). **b.** Quantification of the fluorescent intensity for CPSF proteins (green),
622 DENV NS3 (red) and DAPI (blue) along the indicated line-scans was performed
623 using the Zeiss ZEN software Profile function and plotted on a line graph using
624 Prism. **c.** Immunofluorescence assay of Huh7 cells expressing DENV NS3 showing
625 the intracellular distribution of CPSF3 or CPSF4 (green) with cells expressing NS3
626 indicated by straining with NS3's FLAG tag (red). **d.** Quantification of the fluorescent
627 intensity for CPSF proteins (green), FLAG (red) and DAPI (blue) along the indicated
628 line-scans was performed using the Zeiss ZEN software Profile function and plotted
629 on a line graph using Prism. For b and d, thirty individual data points of the
630 fluorescent intensity for the CPSF proteins were taken from the middle of the nucleus
631 and cytoplasm, and compared by multiple unpaired t-tests and a p-value less than
632 0.05 was considered significant (*, $p < 0.05$; ***, $p < 0.001$; ****, $p < 0.0001$). The
633 images are representative of similar results from three independent biological
634 experiments.
635
636 **Fig. 6. The CPSF complex, but not its endonuclease activity, is critical for**
637 **DENV replication. a**. Bar graph (left) and dot plot (right) showing the relative levels
638 of DENV genomic RNA and DENV plaque forming units (PFU) in Huh7 cells treated
639 with the indicated siRNAs at 40μM for 24h before being infected with DENV for 24h.
640 **b.** Bar graph (left) and dot plot (center) showing the relative levels of DENV genomic
641 RNA and DENV plaque forming units (PFU) in Huh7 cells treated with increasing
642 concentrations of siCPSF3-10. Bar graph showing the relative levels of CPSF3
643 mRNA and Western blot with the indicated antibodies showing the protein levels of
644 DENV NS5 and CPSF3 (right). **c**. Bar graph (left) and dot plot (right) showing the
645 relative levels of ZIKV genomic RNA and ZIKV plaque forming units (PFU) in Huh7
646 cells treated with the indicated siRNAs at 40μM for 24h before being infected with
647 ZIKV for 24h. **d**. V5 immunoprecipitation of 293T cells transfected with FLAG-tagged
648 ZIKV or DENV NS3 and V5-tagged CPSF3, followed by Western blotting with the
649 indicated antibodies, showing that ZIKV NS3, like DENV NS3, interacts with CPSF3.
650 **e.** Bar graph showing the relative cell viability of Huh7 cells treated with the indicated
651 concentrations of JTE-607. **f**. Line graph showing the relative DENV infectivity of
652 Huh7 cells treated with the indicated concentrations of JTE-607. The number of
653 plaque forming units were counted for each sample and plotted relative to the
654 untreated sample. The estimated EC_{50} was calculated using Prism. Western blot
655 with the indicated antibodies of the corresponding cell lysate samples showing the
656 decrease in protein levels of DENV NS5, CPSF3, CPSF4 and actin with treatment of
657 increasing concentrations of JTE-607. Mean values were compared to the respective
658 control samples by Dunnett multiple comparison after one-way ANOVA, and a p-
659 value less than 0.05 was considered significant (*, $p < 0.05$; **, $p < 0.01$; ****, $p <$
660 0.0001).
661
662 **Extended Data Fig. 1. DENV NS1 does not alter the subcellular localization of**
663 **CPSF proteins. a**. Immunofluorescence assay of DENV-infected Huh7 cells
664 showing the intracellular distribution of CPSF4 (green) with infected cells indicated

665 by staining with dsRNA (red). Quantification of the fluorescent intensity for CPSF
666 proteins (green), dsRNA (red) and DAPI (blue) along the indicated line-scans was
667 performed using the Zeiss ZEN software Profile function and plotted on a line graph
668 using Prism (right). **b.** Immunofluorescence assay of Huh7 cells expressing DENV
669 NS1 showing the levels of CPSF4 (green) in the nuclei of cells stained for the FLAG
670 tag on NS1 (red). Quantification of the fluorescent intensity for CPSF proteins
671 (green), FLAG (red) and DAPI (blue) along the indicated line-scans was performed
672 using the Zeiss ZEN software Profile function and plotted on a line graph using Prism
673 (right). Thirty individual data points of the fluorescent intensity for the CPSF proteins
674 were taken from the middle of the nucleus and cytoplasm, and compared by multiple
675 unpaired t-tests and a p-value less than 0.05 was considered significant (****, $p <$
676 0.0001). The images are representative of similar results from three independent
677 biological experiments.
678
679 **Extended Data Fig. 2. DENV NS3 does not affect CPSF complex function.** Bar
680 graph showing the relative levels of IL8 pre-mRNA in Huh7 cells treated and
681 transfected as indicated (top). Results are from two biologically independent
682 experiments with the statistical significance calculated by comparing mean values to
683 the control samples by Dunnett multiple comparison after one-way ANOVA. A p-
684 value less than 0.05 was considered significant (****, $p < 0.0001$). Western blot with
685 the indicated antibodies showing the expression of NS3 and/or NS5 (bottom) is
686 representative of two biologically independent experiments repeated with similar
687 results.
688
689 **Extended Data Fig. 3. The CCT complex interacts specifically with DENV NS1.**
690 **a**. Heat map depicting the average CRAPome scores of the detected CCT complex
691 members from the biological replicates of each bait DENV protein. **b.** Bar graph
692 showing the enriched terms associated with all identified NS1 interacting proteins.
693 Metascape analysis was performed as in Figure 2. **c.** Protein-protein interaction
694 network showing the interactions between DENV NS1 and its PIPs. **d.** FLAG
695 immunoprecipitation of 293T cells transfected with the indicated FLAG-tagged DENV
696 proteins and V5-tagged CCT complex members, followed by Western blotting with
697 the indicated antibodies, showing a specific interaction between the CCT complex
698 and DENV NS1.
699
700 **Extended Data Fig. 4. The helicase domain of DENV NS3 is necessary and**
701 **sufficient to bind the N-terminal of CPSF3.** Immunoprecipitation using the
702 indicated antibodies of 293T cells transfected with FLAG-tagged NS3 and V5-tagged
703 CPSF3, followed by Western blotting with the indicated antibodies. The amino acid
704 positions for the various domains for DENV NS3 and CPSF3 used are depicted.
705
706 **REFERENCES**
707
708 1. Bhatt S, Gething PW, Brady OJ, Messina JP, Farlow AW, Moyes CL, et al. The global
709 distribution and burden of dengue. Nature. 2013;496(7446):504-7.
710 2. Ashburn PM, Craig CF. Experimental Inverstigations Regarding the Etiology of
711 Dengue Fever. The Journal of Infectious Diseases. 1907;4(3):440-75.
712 3. Kuno G, Chang GJ. Full-length sequencing and genomic characterization of
713 Bagaza, Kedougou, and Zika viruses. Archives of virology. 2007;152(4):687-96.

714 4. Marceau CD, Puschnik AS, Majzoub K, Ooi YS, Brewer SM, Fuchs G, et al. Genetic
715 dissection of Flaviviridae host factors through genome-scale CRISPR screens. Nature.
716 2016;535(7610):159-63.
717 5. Lin DL, Cherepanova NA, Bozzacco L, MacDonald MR, Gilmore R, Tai AW. Dengue
718 Virus Hijacks a Noncanonical Oxidoreductase Function of a Cellular
719 Oligosaccharyltransferase Complex. mBio. 2017;8(4).
720 6. Labeau A, Simon-Loriere E, Hafirassou ML, Bonnet-Madin L, Tessier S,
721 Zamborlini A, et al. A Genome-Wide CRISPR-Cas9 Screen Identifies the Dolichol-
722 Phosphate Mannose Synthase Complex as a Host Dependency Factor for Dengue Virus
723 Infection. J Virol. 2020;94(7).
724 7. Savidis G, McDougall WM, Meraner P, Perreira JM, Portmann JM, Trincucci G, et
725 al. Identification of Zika Virus and Dengue Virus Dependency Factors using Functional
726 Genomics. Cell Rep. 2016;16(1):232-46.
727 8. Khadka S, Vangeloff AD, Zhang C, Siddavatam P, Heaton NS, Wang L, et al. A
728 physical interaction network of dengue virus and human proteins. Mol Cell Proteomics.
729 2011;10(12):M111 012187.
730 9. Mairiang D, Zhang H, Sodja A, Murali T, Suriyaphol P, Malasit P, et al.
731 Identification of new protein interactions between dengue fever virus and its hosts,
732 human and mosquito. PLoS One. 2013;8(1):e53535.
733 10. Colpitts TM, Barthel S, Wang P, Fikrig E. Dengue virus capsid protein binds core
734 histones and inhibits nucleosome formation in human liver cells. PLoS One.
735 2011;6(9):e24365.
736 11. Shah PS, Link N, Jang GM, Sharp PP, Zhu T, Swaney DL, et al. Comparative
737 Flavivirus-Host Protein Interaction Mapping Reveals Mechanisms of Dengue and Zika
738 Virus Pathogenesis. Cell. 2018;175(7):1931-45.e18.
739 12. Xie X, Zou J, Wang QY, Shi PY. Targeting dengue virus NS4B protein for drug
740 discovery. Antiviral Res. 2015;118:39-45.
741 13. Heaton NS, Moshkina N, Fenouil R, Gardner TJ, Aguirre S, Shah PS, et al. Targeting
742 Viral Proteostasis Limits Influenza Virus, HIV, and Dengue Virus Infection. Immunity.
743 2016;44(1):46-58.
744 14. Wang L, Fu B, Li W, Patil G, Liu L, Dorf ME, et al. Comparative influenza protein
745 interactomes identify the role of plakophilin 2 in virus restriction. Nat Commun.
746 2017;8:13876.
747 15. Perry JW, Chen Y, Speliotes E, Tai AW. Functional Analysis of the Dengue Virus
748 Genome Using an Insertional Mutagenesis Screen. J Virol. 2018;92(7).
749 16. Aubry F, Nougairede A, Gould EA, de Lamballerie X. Flavivirus reverse genetic
750 systems, construction techniques and applications: a historical perspective. Antiviral
751 Res. 2015;114:67-85.
752 17. Baker C, Shi PY. Construction of Stable Reporter Flaviviruses and Their
753 Applications. Viruses. 2020;12(10).
754 18. Hafirassou ML, Meertens L, Umana-Diaz C, Labeau A, Dejarnac O, Bonnet-Madin
755 L, et al. A Global Interactome Map of the Dengue Virus NS1 Identifies Virus Restriction
756 and Dependency Host Factors. Cell Rep. 2017;21(13):3900-13.
757 19. De Maio FA, Risso G, Iglesias NG, Shah P, Pozzi B, Gebhard LG, et al. The Dengue
758 Virus NS5 Protein Intrudes in the Cellular Spliceosome and Modulates Splicing. PLoS
759 Pathog. 2016;12(8):e1005841.
760 20. Tan MJA, Chan KWK, Ng IHW, Kong SYZ, Gwee CP, Watanabe S, et al. The
761 Potential Role of the ZIKV NS5 Nuclear Spherical-Shell Structures in Cell Type-Specific
762 Host Immune Modulation during ZIKV Infection. Cells. 2019;8(12).

763 21. Stern O, Hung YF, Valdau O, Yaffe Y, Harris E, Hoffmann S, et al. An N-terminal
764 amphipathic helix in dengue virus nonstructural protein 4A mediates oligomerization
765 and is essential for replication. J Virol. 2013;87(7):4080-5.
766 22. Fajardo-Sanchez E, Galiano V, Villalain J. Spontaneous membrane insertion of a
767 dengue virus NS2A peptide. Arch Biochem Biophys. 2017;627:56-66.
768 23. Bachmair A, Finley D, Varshavsky A. In vivo half-life of a protein is a function of
769 its amino-terminal residue. Science. 1986;234(4773):179-86.
770 24. Varshavsky A. Ubiquitin fusion technique and its descendants. Methods Enzymol.
771 2000;327:578-93.
772 25. Choi H, Larsen B, Lin ZY, Breitkreutz A, Mellacheruvu D, Fermin D, et al. SAINT:
773 probabilistic scoring of affinity purification-mass spectrometry data. Nat Methods.
774 2011;8(1):70-3.
775 26. Mellacheruvu D, Wright Z, Couzens AL, Lambert JP, St-Denis NA, Li T, et al. The
776 CRAPome: a contaminant repository for affinity purification-mass spectrometry data.
777 Nat Methods. 2013;10(8):730-6.
778 27. Brooks AJ, Johansson M, John AV, Xu Y, Jans DA, Vasudevan SG. The interdomain
779 region of dengue NS5 protein that binds to the viral helicase NS3 contains
780 independently functional importin beta 1 and importin alpha/beta-recognized nuclear
781 localization signals. J Biol Chem. 2002;277(39):36399-407.
782 28. Johansson M, Brooks AJ, Jans DA, Vasudevan SG. A small region of the dengue
783 virus-encoded RNA-dependent RNA polymerase, NS5, confers interaction with both the
784 nuclear transport receptor importin-beta and the viral helicase, NS3. J Gen Virol.
785 2001;82(Pt 4):735-45.
786 29. Zou J, Xie X, Wang QY, Dong H, Lee MY, Kang C, et al. Characterization of dengue
787 virus NS4A and NS4B protein interaction. J Virol. 2015;89(7):3455-70.
788 30. Tan MJA, Brown NG, Chan KWK, Jin JY, Zu Kong SY, Vasudevan SG. Mutations in
789 the cytoplasmic domain of dengue virus NS4A affect virus fitness and interactions with
790 other non-structural proteins. J Gen Virol. 2020;101(9):941-53.
791 31. Plaszczyca A, Scaturro P, Neufeldt CJ, Cortese M, Cerikan B, Ferla S, et al. A novel
792 interaction between dengue virus nonstructural protein 1 and the NS4A-2K-4B
793 precursor is required for viral RNA replication but not for formation of the membranous
794 replication organelle. PLoS Pathog. 2019;15(5):e1007736.
795 32. Xie X, Zou J, Zhang X, Zhou Y, Routh AL, Kang C, et al. Dengue NS2A Protein
796 Orchestrates Virus Assembly. Cell Host Microbe. 2019;26(5):606-22 e8.
797 33. Lescar J, Soh S, Lee LT, Vasudevan SG, Kang C, Lim SP. The Dengue Virus
798 Replication Complex: From RNA Replication to Protein-Protein Interactions to Evasion
799 of Innate Immunity. Adv Exp Med Biol. 2018;1062:115-29.
800 34. Li M, Johnson JR, Truong B, Kim G, Weinbren N, Dittmar M, et al. Identification of
801 antiviral roles for the exon-junction complex and nonsense-mediated decay in flaviviral
802 infection. Nat Microbiol. 2019;4(6):985-95.
803 35. Tay MY, Smith K, Ng IH, Chan KW, Zhao Y, Ooi EE, et al. The C-terminal 18 Amino
804 Acid Region of Dengue Virus NS5 Regulates its Subcellular Localization and Contains a
805 Conserved Arginine Residue Essential for Infectious Virus Production. PLoS Pathog.
806 2016;12(9):e1005886.
807 36. Barbier V, Lang D, Valois S, Rothman AL, Medin CL. Dengue virus induces
808 mitochondrial elongation through impairment of Drp1-triggered mitochondrial fission.
809 Virology. 2017;500:149-60.

810 37. Chatel-Chaix L, Cortese M, Romero-Brey I, Bender S, Neufeldt CJ, Fischl W, et al.
811 Dengue Virus Perturbs Mitochondrial Morphodynamics to Dampen Innate Immune
812 Responses. Cell Host Microbe. 2016;20(3):342-56.
813 38. Puschnik AS, Marceau CD, Ooi YS, Majzoub K, Rinis N, Contessa JN, et al. A Small-
814 Molecule Oligosaccharyltransferase Inhibitor with Pan-flaviviral Activity. Cell Rep.
815 2017;21(11):3032-9.
816 39. Romero-Brey I, Bartenschlager R. Endoplasmic Reticulum: The Favorite
817 Intracellular Niche for Viral Replication and Assembly. Viruses. 2016;8(6).
818 40. Arakawa M, Morita E. Flavivirus Replication Organelle Biogenesis in the
819 Endoplasmic Reticulum: Comparison with Other Single-Stranded Positive-Sense RNA
820 Viruses. Int J Mol Sci. 2019;20(9).
821 41. Mandel CR, Kaneko S, Zhang H, Gebauer D, Vethantham V, Manley JL, et al.
822 Polyadenylation factor CPSF-73 is the pre-mRNA 3'-end-processing endonuclease.
823 Nature. 2006;444(7121):953-6.
824 42. Liu H, Moore CL. On the Cutting Edge: Regulation and Therapeutic Potential of
825 the mRNA 3' End Nuclease. Trends Biochem Sci. 2021;46(9):772-84.
826 43. Wang X, Hennig T, Whisnant AW, Erhard F, Prusty BK, Friedel CC, et al. Herpes
827 simplex virus blocks host transcription termination via the bimodal activities of ICP27.
828 Nat Commun. 2020;11(1):293.
829 44. Kakegawa J, Sakane N, Suzuki K, Yoshida T. JTE-607, a multiple cytokine
830 production inhibitor, targets CPSF3 and inhibits pre-mRNA processing. Biochem
831 Biophys Res Commun. 2019;518(1):32-7.
832 45. Ross NT, Lohmann F, Carbonneau S, Fazal A, Weihofen WA, Gleim S, et al. CPSF3-
833 dependent pre-mRNA processing as a druggable node in AML and Ewing's sarcoma. Nat
834 Chem Biol. 2020;16(1):50-9.
835 46. Kaptein SJF, Goethals O, Kiemel D, Marchand A, Kesteleyn B, Bonfanti JF, et al.
836 Publisher Correction: A pan-serotype dengue virus inhibitor targeting the NS3-NS4B
837 interaction. Nature. 2021;599(7883):E2.
838 47. Watanabe S, Tan NWW, Chan KWK, Vasudevan SG. Dengue Virus and Zika Virus
839 Serological Cross-reactivity and Their Impact on Pathogenesis in Mice. J Infect Dis.
840 2019;219(2):223-33.
841 48. Low JG, Ooi EE, Tolfvenstam T, Leo YS, Hibberd ML, Ng LC, et al. Early Dengue
842 infection and outcome study (EDEN) - study design and preliminary findings. Ann Acad
843 Med Singap. 2006;35(11):783-9.
844 49. Yang X, Boehm JS, Yang X, Salehi-Ashtiani K, Hao T, Shen Y, et al. A public
845 genome-scale lentiviral expression library of human ORFs. Nat Methods. 2011;8(8):659-
846 61.
847 50. Moreland NJ, Tay MY, Lim E, Rathore AP, Lim AP, Hanson BJ, et al. Monoclonal
848 antibodies against dengue NS2B and NS3 proteins for the study of protein interactions
849 in the flaviviral replication complex. J Virol Methods. 2012;179(1):97-103.
850 51. Collins TJ. ImageJ for microscopy. BioTechniques. 2007;43(1 Suppl):25-30.
851 52. Shannon P, Markiel A, Ozier O, Baliga NS, Wang JT, Ramage D, et al. Cytoscape: a
852 software environment for integrated models of biomolecular interaction networks.
853 Genome Res. 2003;13(11):2498-504.
854 53. Zhou Y, Zhou B, Pache L, Chang M, Khodabakhshi AH, Tanaseichuk O, et al.
855 Metascape provides a biologist-oriented resource for the analysis of systems-level
856 datasets. Nat Commun. 2019;10(1):1523.
857

Figure 1

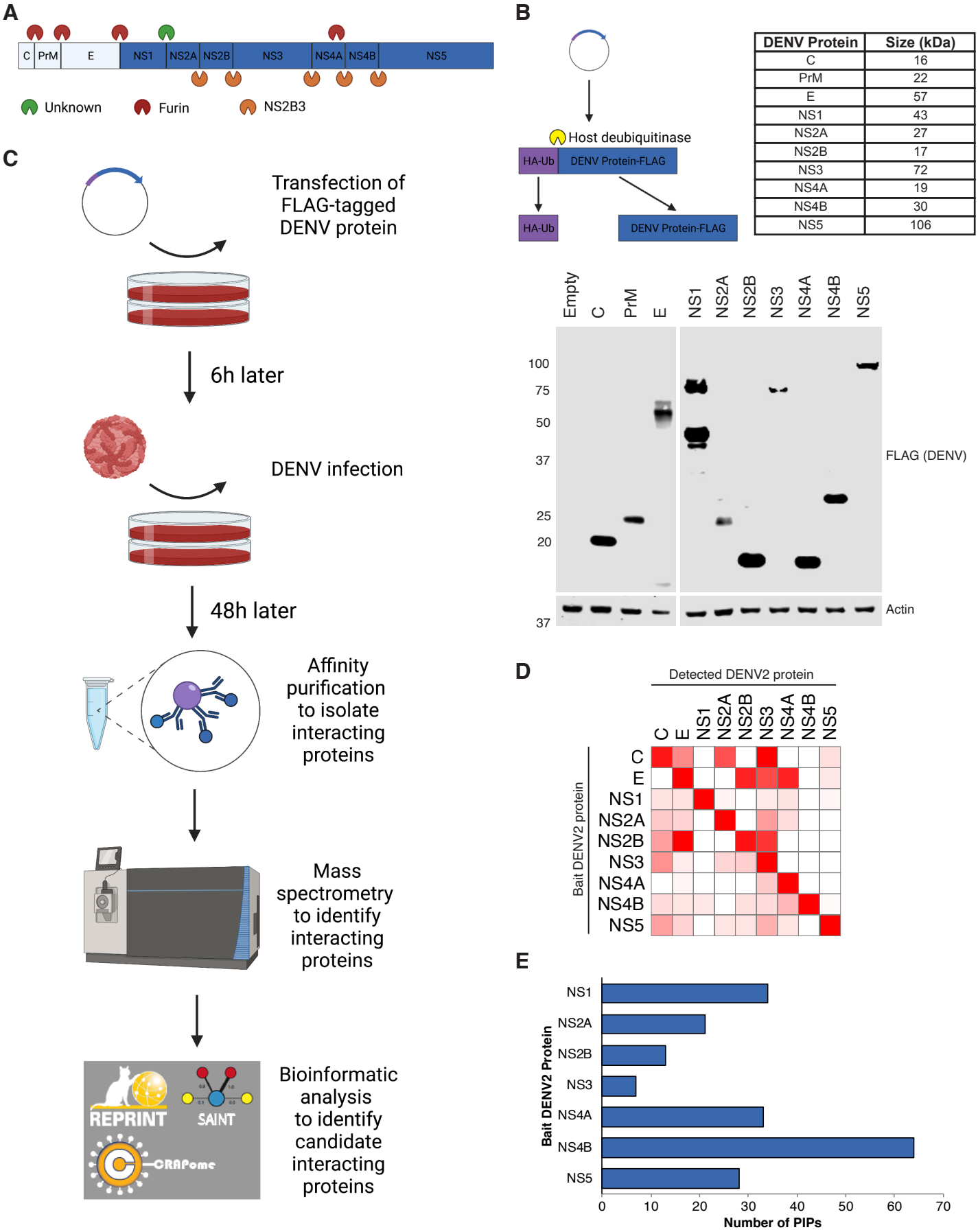

DENV Protein	Size (kDa)
C	16
PrM	22
E	57
NS1	43
NS2A	27
NS2B	17
NS3	72
NS4A	19
NS4B	30
NS5	106

Figure 2

A

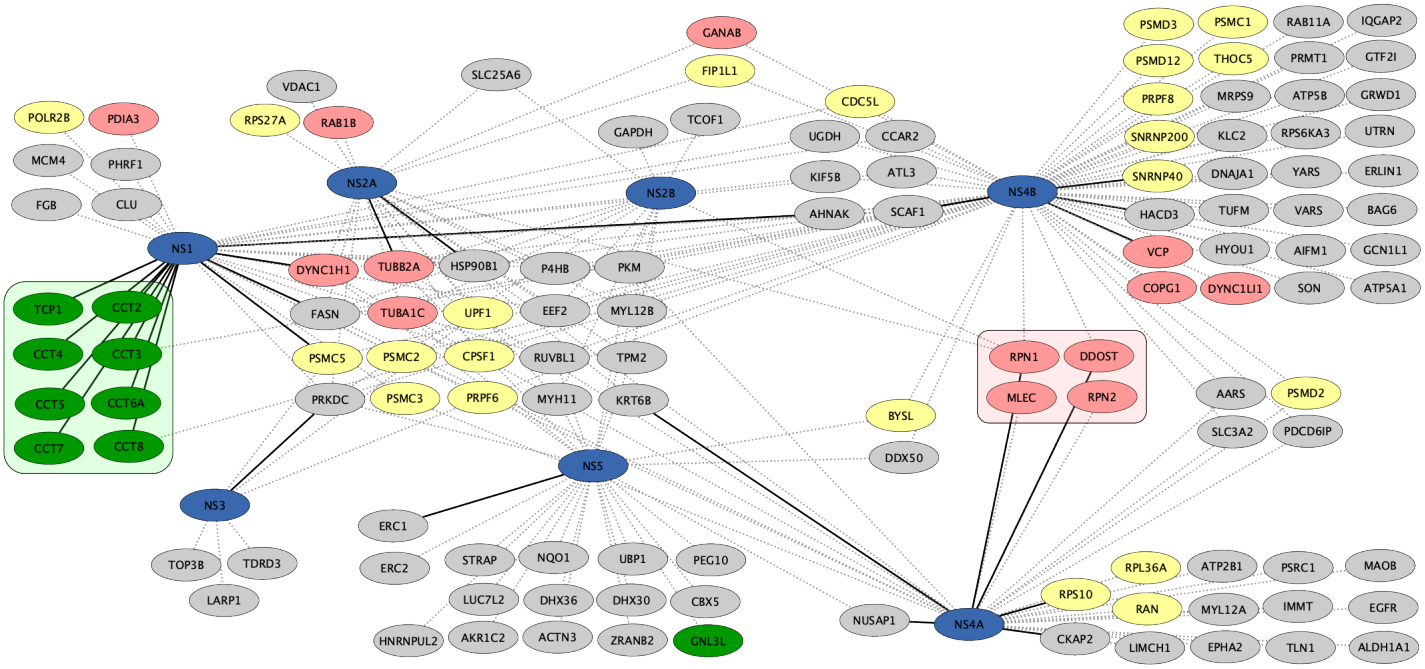

B

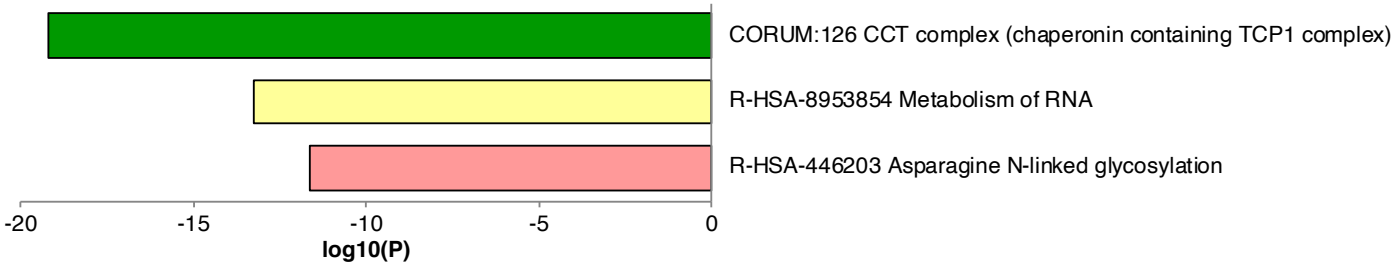

C

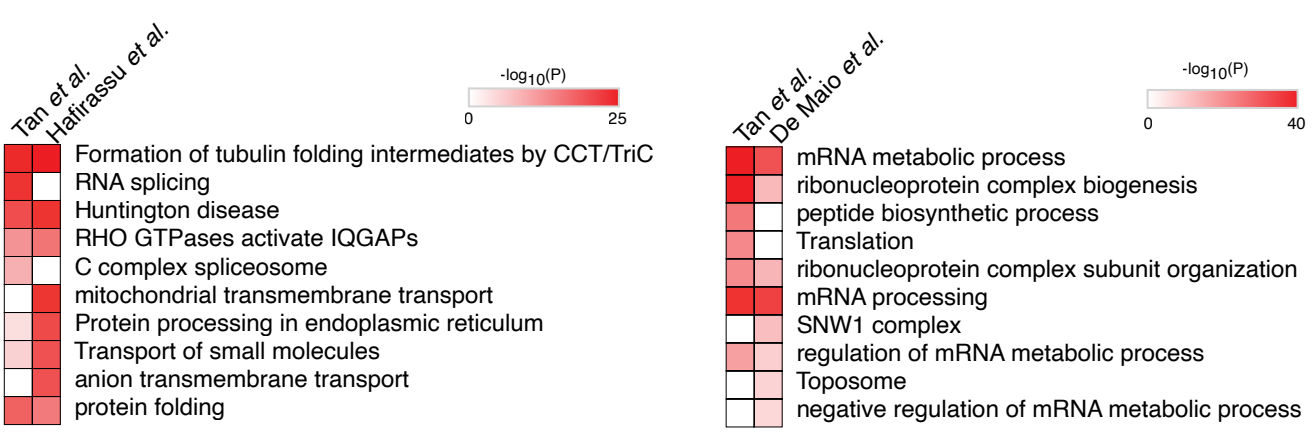

D

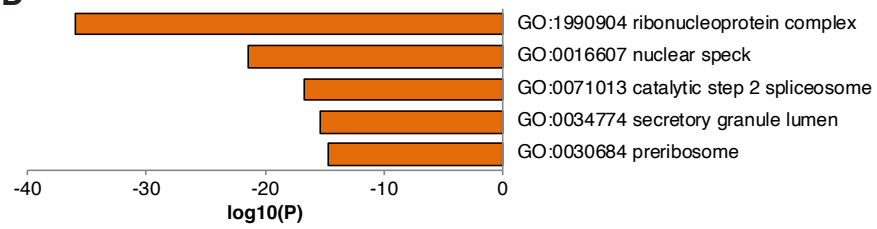

E

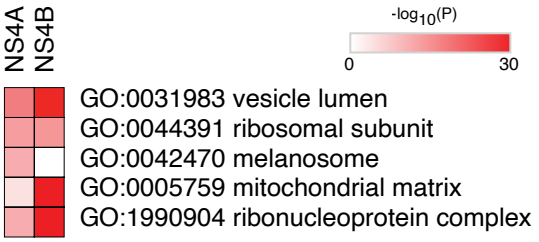

Figure 3

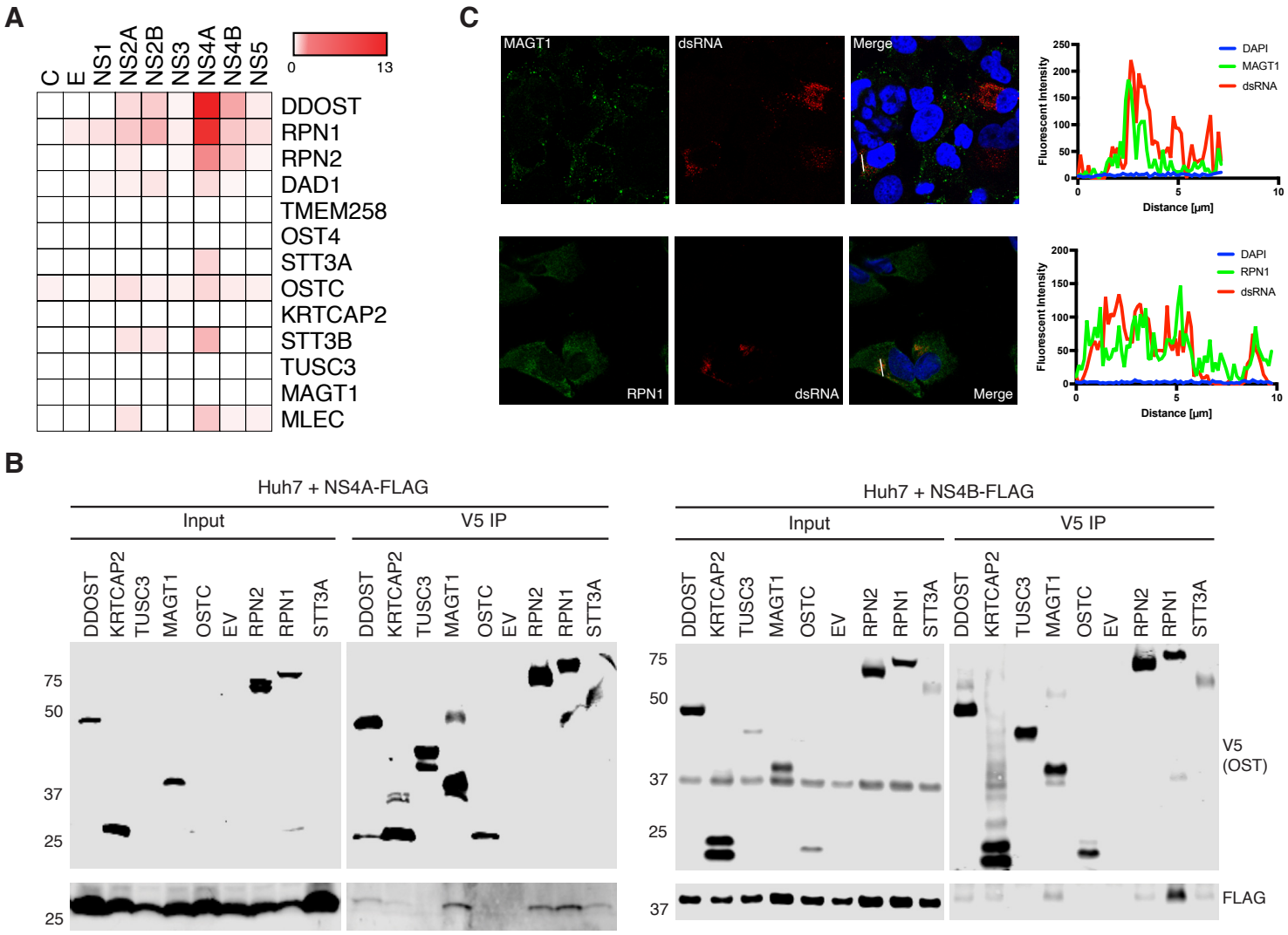
A
C
E
NS1
NS2A
NS2B
NS3
NS4A
NS4B
NS5
0
13
DDOST
RPN1
RPN2
DAD1
TMEM258
OST4
STT3A
OSTC
KRTCAP2
STT3B
TUSC3
MAGT1
MLEC
C
MAGT1
dsRNA
Merge
Fluorescent Intensity
Distance [µm]
DAPI
MAGT1
dsRNA
RPN1
dsRNA
Merge
Fluorescent Intensity
Distance [µm]
DAPI
RPN1
dsRNA
B
Huh7 + NS4A-FLAG
Input
V5 IP
DDOST
KRTCAP2
TUSC3
MAGT1
OSTC
EV
RPN2
RPN1
STT3A
75
50
37
25
25
Huh7 + NS4B-FLAG
Input
V5 IP
DDOST
KRTCAP2
TUSC3
MAGT1
OSTC
EV
RPN2
RPN1
STT3A
75
50
37
25
37
V5
(OST)
FLAG

Figure 4

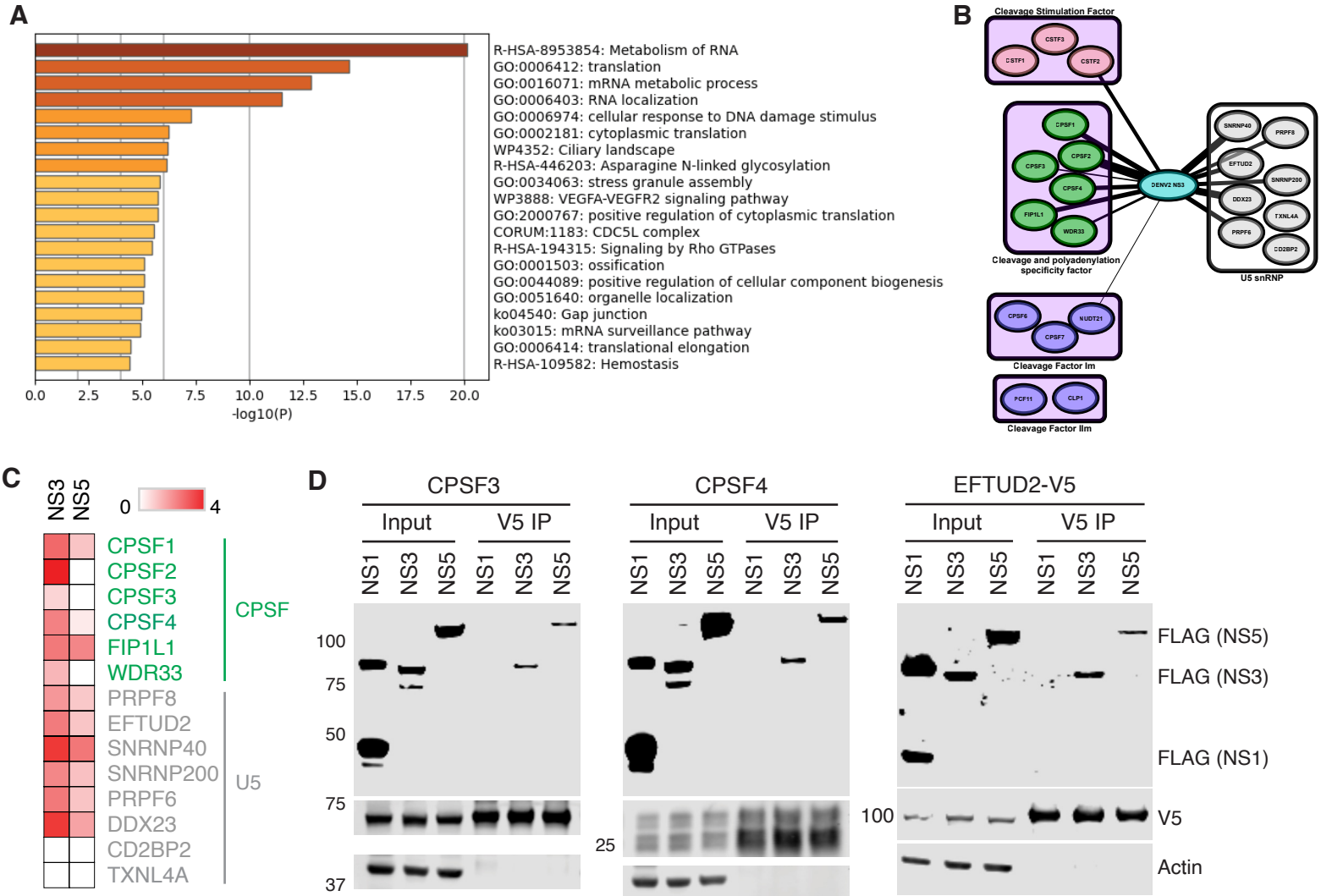
A
R-HSA-8953854: Metabolism of RNA
GO:0006412: translation
GO:0016071: mRNA metabolic process
GO:0006403: RNA localization
GO:0006974: cellular response to DNA damage stimulus
GO:0002181: cytoplasmic translation
WP4352: Ciliary landscape
R-HSA-446203: Asparagine N-linked glycosylation
GO:0034063: stress granule assembly
WP3888: VEGFA-VEGFR2 signaling pathway
GO:2000767: positive regulation of cytoplasmic translation
CORUM:1183: CDC5L complex
R-HSA-194315: Signaling by Rho GTPases
GO:0001503: ossification
GO:0044089: positive regulation of cellular component biogenesis
GO:0051640: organelle localization
ko04540: Gap junction
ko03015: mRNA surveillance pathway
GO:0006414: translational elongation
R-HSA-109582: Hemostasis
0.0 2.5 5.0 7.5 10.0 12.5 15.0 17.5 20.0
-log10(P)
B
Cleavage Stimulation Factor
CSTF3
CSTF1
CSTF2
CPSF1
CPSF2
CPSF3
CPSF4
FIP1L1
WDR33
Cleavage and polyadenylation specificity factor
DENV2 NS3
SNRNP40
PRPF8
EFTUD2
SNRNP200
DDX23
TXNL4A
PRPF6
CD2BP2
U5 snRNP
CPSF6
NUDT21
CPSF7
Cleavage Factor Im
PCF11
CLP1
Cleavage Factor IIm
C
NS3
NS5
0
4
CPSF1
CPSF2
CPSF3
CPSF4
FIP1L1
WDR33
CPSF
PRPF8
EFTUD2
SNRNP40
SNRNP200
PRPF6
DDX23
CD2BP2
TXNL4A
U5
D
CPSF3
CPSF4
EFTUD2-V5
Input
V5 IP
NS1
NS3
NS5
100
75
50
75
37
25
100
FLAG (NS5)
FLAG (NS3)
FLAG (NS1)
V5
Actin

Figure 5

A

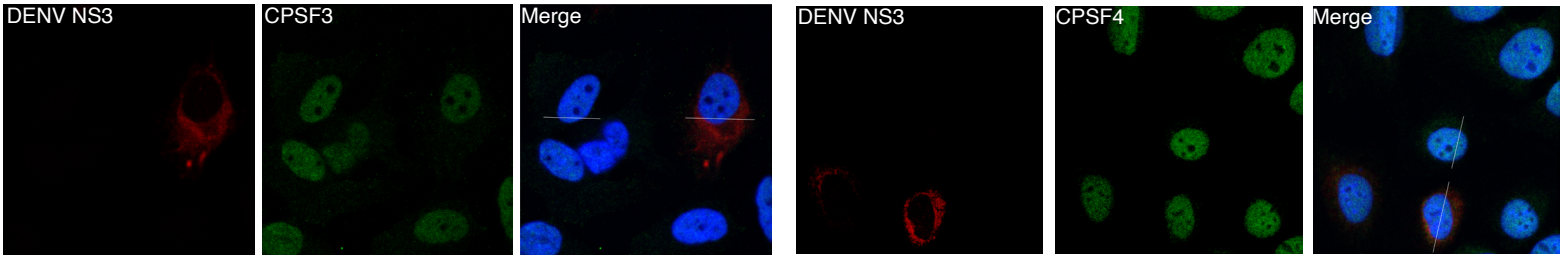

B

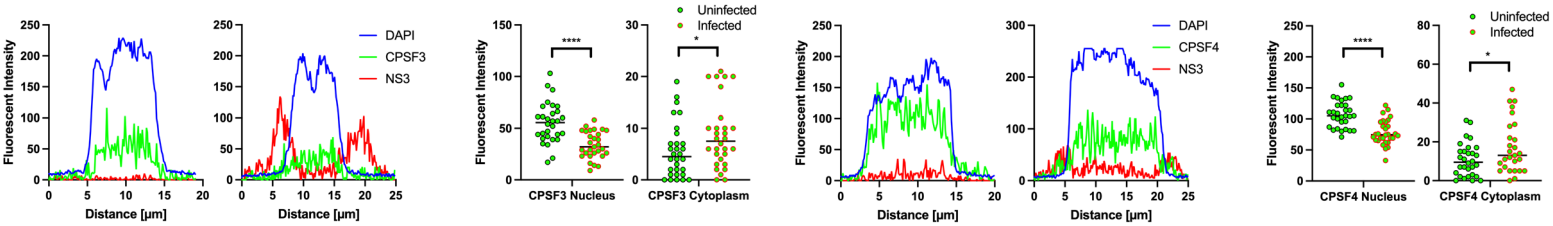

C

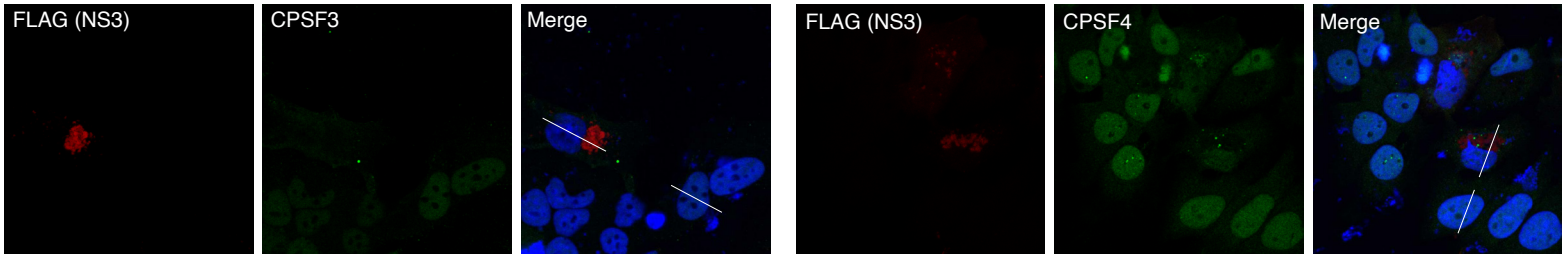

D

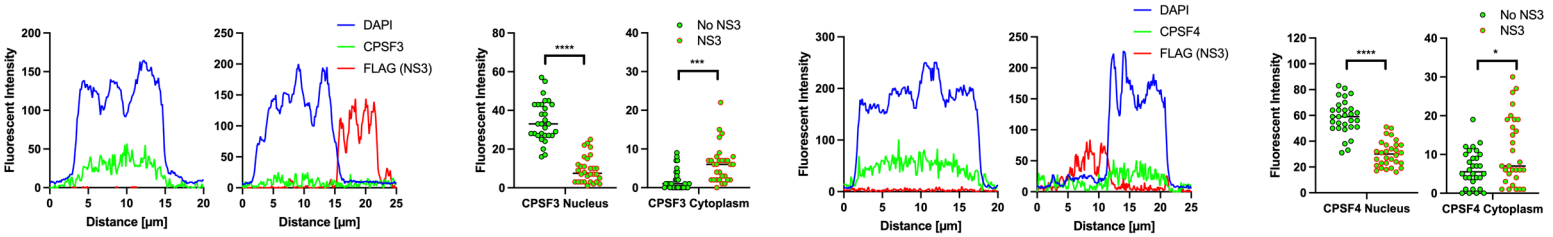

Figure 6

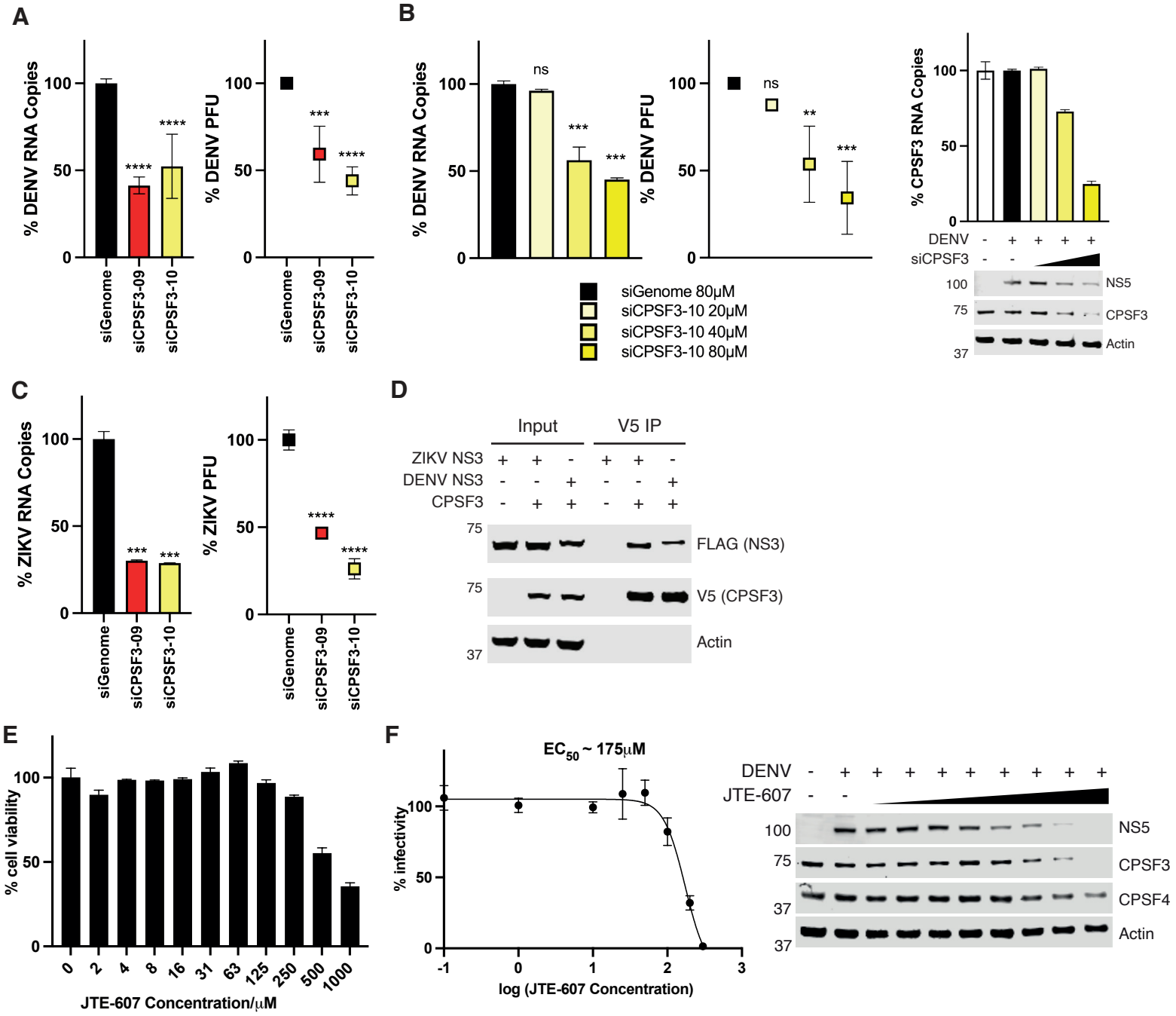
A
% DENV RNA Copies
% DENV PFU
siGenome
siCPSF3-09
siCPSF3-10
B
% DENV RNA Copies
% DENV PFU
ns
siGenome 80μM
siCPSF3-10 20μM
siCPSF3-10 40μM
siCPSF3-10 80μM
% CPSF3 RNA Copies
DENV
siCPSF3
NS5
CPSF3
Actin
C
% ZIKV RNA Copies
% ZIKV PFU
D
Input
V5 IP
ZIKV NS3
DENV NS3
CPSF3
FLAG (NS3)
V5 (CPSF3)
Actin
E
% cell viability
JTE-607 Concentration/μM
F
EC50 ~ 175μM
% infectivity
log (JTE-607 Concentration)
DENV
JTE-607
NS5
CPSF3
CPSF4
Actin

Extended Data Figure 1

A

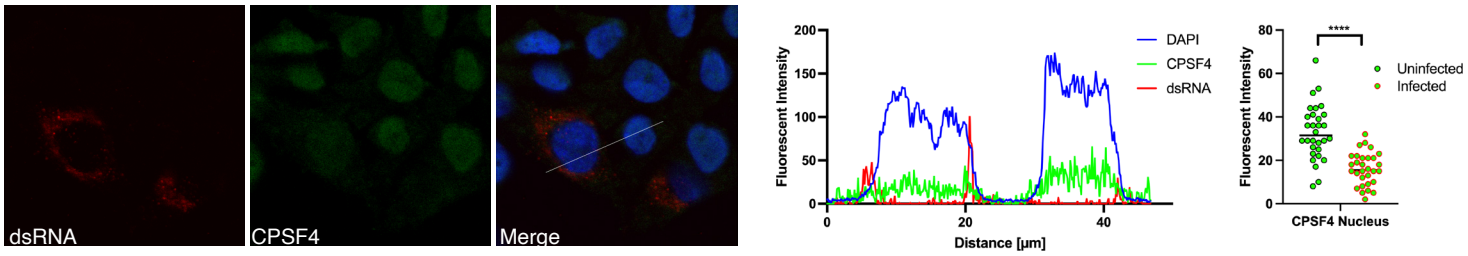

B

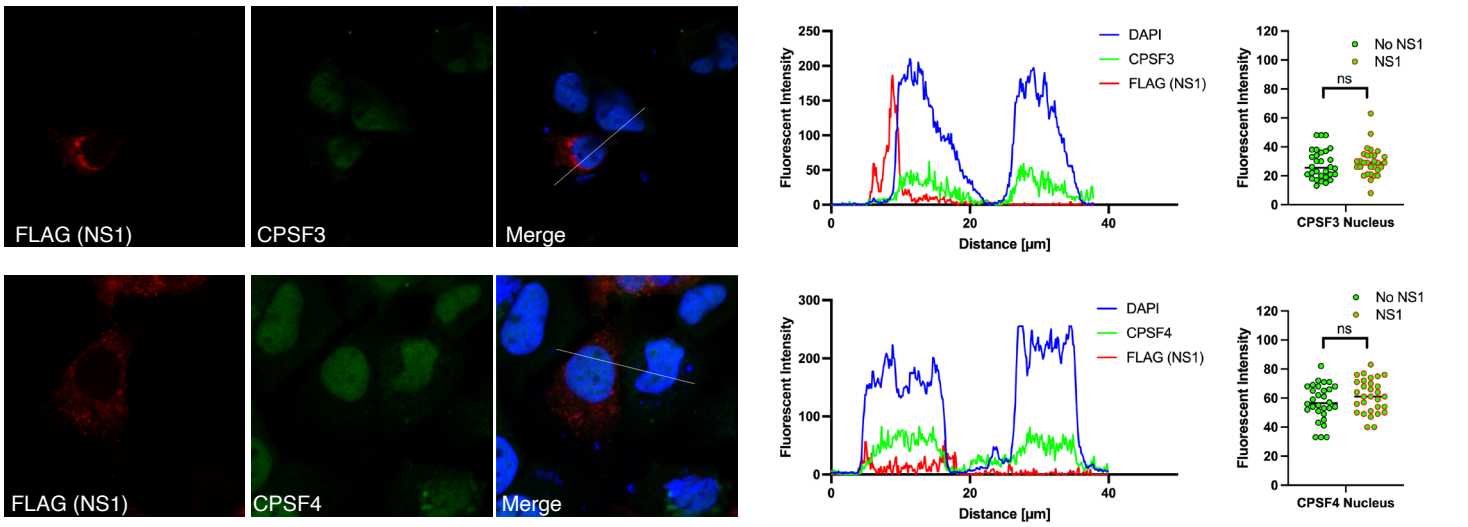

Extended Data Figure 2

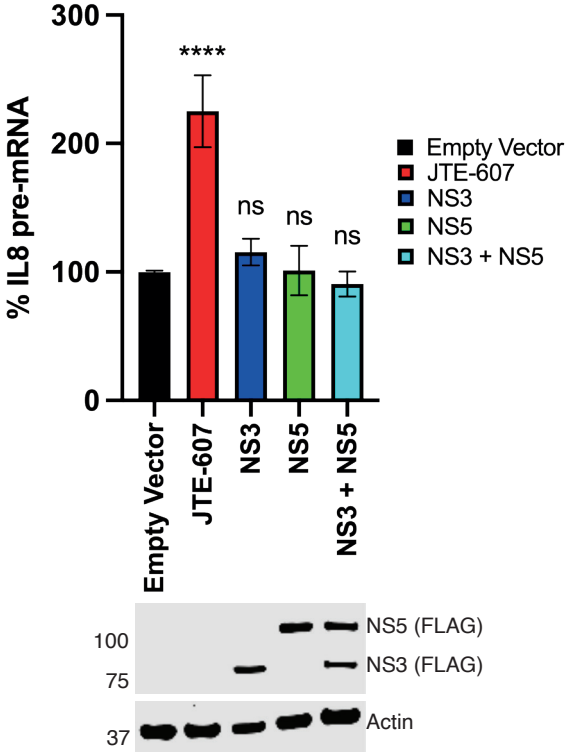

Extended Data Figure 3

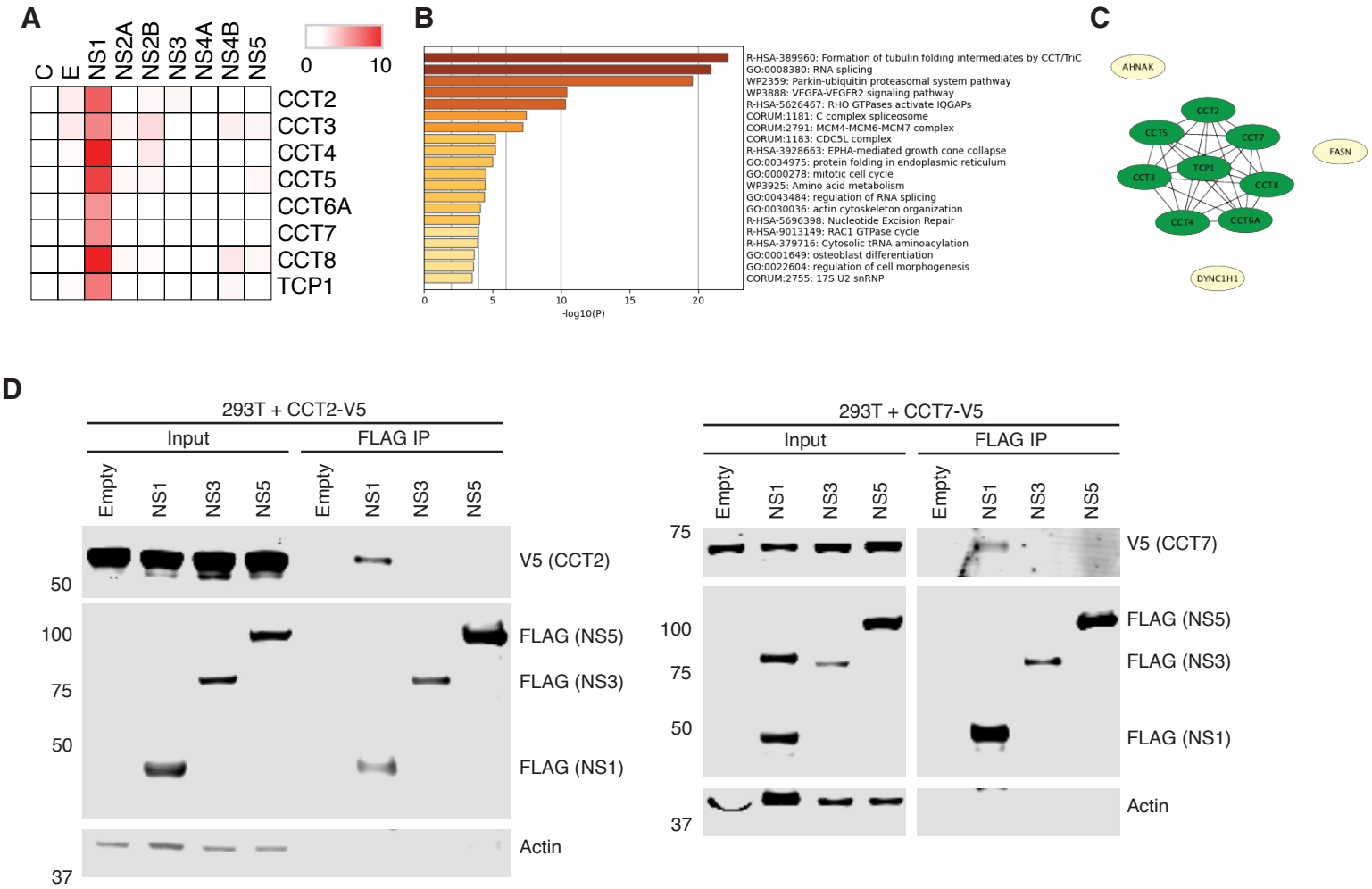
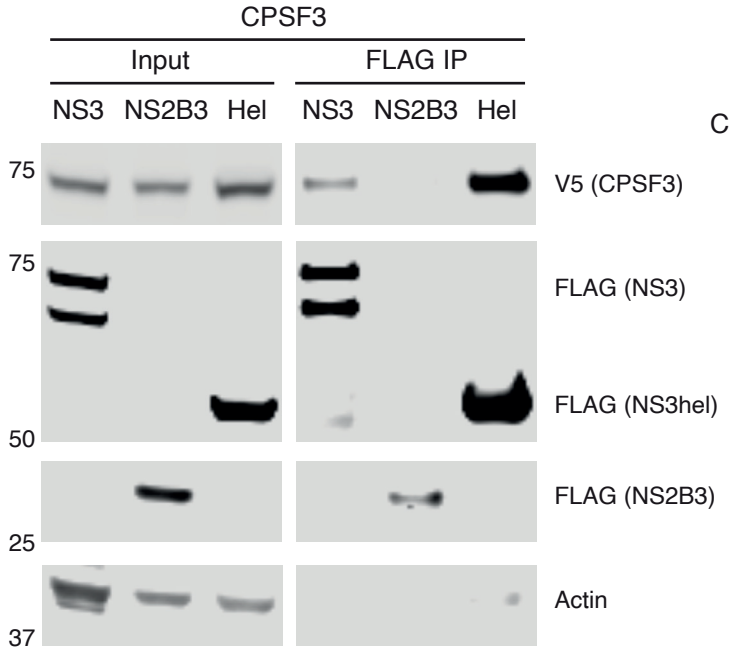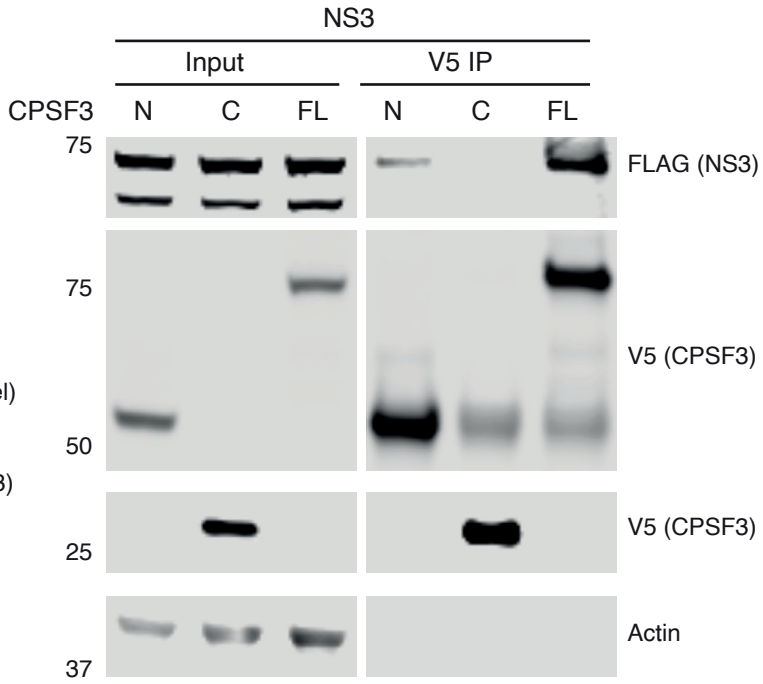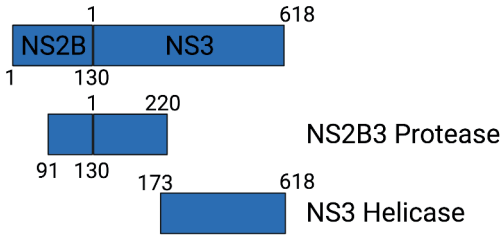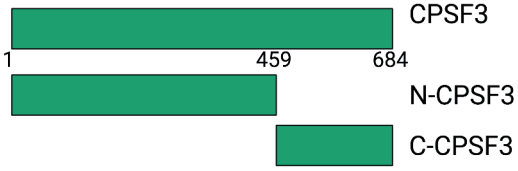
Extended Data Figure 4